

**GASEOUS SWELLING AND RELEASE IN NUCLEAR FUELS
DURING GRAIN GROWTH**

A Thesis
Presented to
The Academic Faculty

By

Hubert Gibson

In Partial Fulfillment
Of the Requirements for the Degree
Master of Science in Nuclear Engineering
Woodruff School of Mechanical Engineering

Georgia Institute of Technology

August 2013

Copyright © 2013 by Hubert C. Gibson

Gaseous Swelling and Release in Nuclear Fuels during Grain Growth

Approved by:

Dr. Chaitanya Deo
School of Mechanical Engineering
Georgia Institute of Technology

Dr. Bojan Petrovic
School of Mechanical Engineering
Georgia Institute of Technology

Dr. Glenn E. Sjoden
School of Mechanical Engineering
Georgia Institute of Technology

Date Approved: 6/24/2013

ACKNOWLEDGEMENTS

I am grateful to my advisor, Dr. Chaitanya Deo, for his guidance and support. This thesis could not exist without his wisdom.

In addition, my thanks go to Dr. Ali Massih. His timely advice spared days of wasted effort, and I am indebted to his assistance.

TABLE OF CONTENTS

	Page
Acknowledgements	iii
List of Tables	v
List of Figures	vi
Summary	viii
Chapter 1. Introduction	1
Chapter 2. Theory	5
Chapter 3. Methodology	18
Chapter 4. Results	30
Chapter 5. Conclusion	44
Appendix A: Generalized Weight Moment Integrals	47
REFERENCES	48

LIST OF TABLES

	Page
1. UO ₂ Gas Diffusion Parameters	25
2. Fuel Power Density and Other Input Parameters of UO ₂	26
3. Sample Data for Fixed Grain Radius Model for 1900 K	32
4. Sample Data for Grain Growth Gas Diffusion Model for 1900 K.	35

LIST OF FIGURES

	Page
1. Growth of Intergranular Bubbles on Fuel Grain Crystals	2
2. Spherical Fuel Grain Crystal System	6
3. Spherical Fuel Grain Crystal undergoing Crystal Growth	11
4. Dihedral Angle of Lenticular Intergranular Bubbles	14
5. The Diffusivity ($\text{m}^2 \text{s}^{-1}$) of UO_2 over inverse temperature (K^{-1})	26
6. Fuel Grain Size (μm) at 1600 K over Time (hr)	28
7. Fuel Grain Size (μm) at 2200 K over Time (hr)	28
8. Benchmark of Fixed Grain Radius Model	30
9. Intergranular gas density of Fixed Grain Radius Model	31
10. Gaseous Swelling of Fixed Grain Radius Model by Temperature	32
11. Gaseous Swelling of Fixed Grain Radius Model by Radius	33
12. Benchmark of Grain Growth Model	34
13. Intergranular Gas Density (mol m^{-3}) over time (hr) using Jernkvist's and Massih's model of grain growth for UO_2	35
14. Intergranular gas density (mol m^{-3}) over time (hr) using Nichols' fourth power grain growth equation for MOX	36
15. Intergranular gas density (mol m^{-3}) over time (hr) using Sari's cubic grain growth equation for MOX.	36
16. Gaseous Swelling over time (hr) using Jernkvist's and Massih's model of grain growth for UO_2	37
17. Gaseous Swelling over time (hr) using Nichols' fourth power grain growth equation for MOX	38
18. Gaseous Swelling over time (hr) using Sari's cubic grain growth equation for MOX	38

19.	Fractional gas release over time (hr) using Jernkvist's and Massih's model of grain growth for UO_2 by Temperature	39
20.	Fractional gas release using Nichols' fourth power grain growth equation for MOX by Temperature	40
21.	Fractional Gas Release using Sari's cubic grain growth equation for MOX by Temperature	40
22.	Fractional gas release over time (hr) using Jernkvist's and Massih's model of grain growth for UO_2 by Temperature	41
23.	Fractional gas release using Nichols' fourth power grain growth equation for MOX by Temperature	42
24.	Fractional Gas Release using Sari's cubic grain growth equation for MOX by Temperature	42
25.	Fractional Gas Release over time (hr) from UO_2 at 1900 K for arbitrarily scaled diffusivities	43
26.	Gaseous Swelling over time (hr) for UO_2 at 1600 K	44
27.	Gaseous Swelling over time (hr) for UO_2 at 1900 K	45

SUMMARY

The fission chain reaction causes swelling in nuclear fuel pins. A significant portion of this swelling is due to the accumulation of fission gas within the boundaries of the grain of fuel. Over time, the fuel releases the trapped gas to the interior of the fuel rods. High temperature grain growth decreases the total surface area of the fuel grains, which decreases the density of intergranular gas required to escape the fuel. This grain growth also speeds the migration of gas atoms through the fuel due to grain boundary sweeping. This paper presents a model of the generation, migration, and release of fission gas, as well as the total swelling over time. It uses an ideal spherical fuel grain with a time-dependent radius.

UO₂ and quasi-homogeneous MOX fuels were simulated with this model. Gaseous swelling and fission gas release were calculated for temperatures from 1600 K to 2200 K. The grain growth of UO₂ was found to decrease the time needed to saturate the intergranular boundaries as compared to simple diffusion without grain growth. Small temperatures increased the time required for saturation, as did small rates of grain growth. Gaseous swelling was within the range of values found by experimental data.

CHAPTER 1

INTRODUCTION

Due to the fission process, nuclear fuels generate both extreme amounts of heat in proportion to their mass and atomic byproducts within the fuel over time. This causes changes in the size and micro-structure of the fuel. The solid fission products cause perceptible swelling of the fuel pellet, and they diffuse within individual fuel grains, but they tend not to migrate outside of the fuel [1]. The same occurs at temperatures below 1300 K for gaseous fission products, such as Krypton, Xenon, Argon, and other noble gases. At temperatures above 1300 K, gaseous fission products do not remain in solution within UO_2 and other fuels. The atoms congregate into intragranular bubbles within the fuel. These bubbles grow and shrink due to the effects of irradiation-based re-solution of atoms from the bubble to the fuel. The gas atoms migrate over time to the boundaries between fuel grains and join the intergranular bubbles [2]. When the gas in these intergranular bubbles reaches the saturation gas area density, the bubbles interconnect with one another and form a network that extends to the fuel pellet exterior [3]. The network allows fission gas to escape the fuel pellet while increasing its total swelling. Figure 1 shows a representation of the fuel grains and the intergranular bubbles.

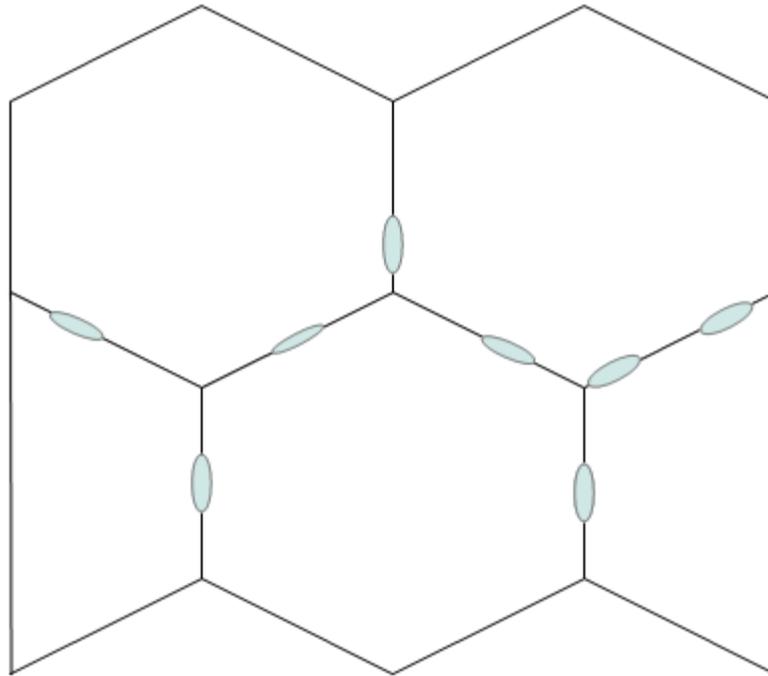


Figure 1. Growth of Intergranular Bubbles on Fuel Grain Crystals. Intergranular Bubbles are shown in gray. Intragranular Bubbles are not shown.

These fission gases are of intense interest in research, due to their various deleterious effects in the nuclear reactor system [1]. The swelling these intergranular gases cause exceeds that of solid fission products. The swelling is large enough to cause the fuel pellet to contact the cladding and increase its stress. In addition, the increase of gases at the fuel boundaries decreases the thermal conductivity of the fuel pin. Due to the already radially heterogeneous nature of the fuel temperature, the fuel expands unevenly, and cracks form within the pin [31]. Fuel cracks that reach the surface acts as stress points when they come in contact with the cladding, due to the effects of friction or adhesion as the fuel tears. As the fuel pin swells, the crack openings increase the local cladding strain. The reduced thermal conductivity due to the intergranular bubble

network exacerbates this phenomenon. In addition, since higher temperatures increases the rate of fission gas release, the decrease in thermal conductivity leads these factors to create a positive feedback loop. Finally, the effects of reactor power transients further modify this swollen system, increasing the risk of fuel cladding failure.

In addition to issues regarding the changed fuel conductivity due to retained gas, the released gas complicates the design process as well. Solid fission products cause swelling due to the distortions they cause the oxide matrix, and they possess various rates of radioactivity, but they remain within the fuel. Fission gases tend to be highly radioactive and are able to migrate to the atmosphere of the cladding [1]. When the cladding fails, the gases enter the primary coolant loop. Removal of these gases from this isolated loop requires a dedicated degasification system [32]. Due to the inert nature of noble gases, the design of this system is complicated. This system is only used as needed; the short half-lives of many of the gases cause decay of the gases to either solid products or stable gas isotopes. The storage and release of these gases to the atmosphere requires careful planning and execution in order to adhere to the requirements and regulations set by the NRC.

At high temperatures, a significant amount of grain growth occurs in nuclear fuels. Fuel grains of different orientations have a higher energy relative to one another, and increased temperatures enable the grains to expand their boundaries to minimize the boundary energy [33]. In this process, larger grains consume smaller grains of similar angular orientations. The rate of consumption decreases as fewer numbers of larger grains with larger differences of orientation develop. The grain growth aids the migration of gas atoms and can exceed the rate of diffusion [4]. However, the increased fuel grain size

decreases the gaseous swelling, due to the reduced interior surface area of the fuel grains [5].

This paper uses the model of gas release during grain growth created by Forsberg and Massih [6], combines it with their later work on gaseous swelling, and extends the model from UO_2 to other fuels. Chapter 2 explains the mathematics underlying two models of gas diffusion through the fuel: one with fixed grain sizes and one with grain growth. This chapter also explains how the grain boundary gas densities lead to the gaseous swelling. Chapter 3 explains the approximations used to solve the models of gas diffusion with a computer. It also lists the parameters of UO_2 and MOX fuels needed during the computer simulation. Chapter 4 discusses the results of the models and of the simulated fuels. Chapter 5 concludes the paper by comparing the scientific literature to the model results.

CHAPTER 2

THEORY

Researchers study the problem of gas generation and diffusion by modeling with a spherical grain of fuel, as shown in Figure 2. Originally, Booth assumed that the escaped gas does not return to the fuel grain [34], which implies a perfect sink condition

$$C(R,t)=0 \tag{1}$$

for a simple diffusion problem [7]. Here, C is the density of gas atoms in m^{-3} , R is the radius of the crystal in m, and t is the time in s.

The diffusion equation, is formulated as a spherical system,

$$\frac{\delta C(r,t)}{\delta t} = D(t)\nabla_r^2 C(r,t) + \beta(t) \tag{2}$$

$$\nabla_r^2 = \frac{\partial^2}{\partial r^2} + \frac{2}{r} \frac{\partial}{\partial r} \tag{3}$$

where the first term in the equation is the diffusion rate of gas atoms, D is the diffusion constant of the gas atoms in $\text{m}^2 \text{s}^{-1}$, and $\beta(t)$ is the gas production rate in $\text{m}^{-3} \text{s}^{-1}$. Matthews and Woods originally solved this equation for time varying temperatures and gas generation rates by using a backwards Euler approximation for a two-region sphere [35].

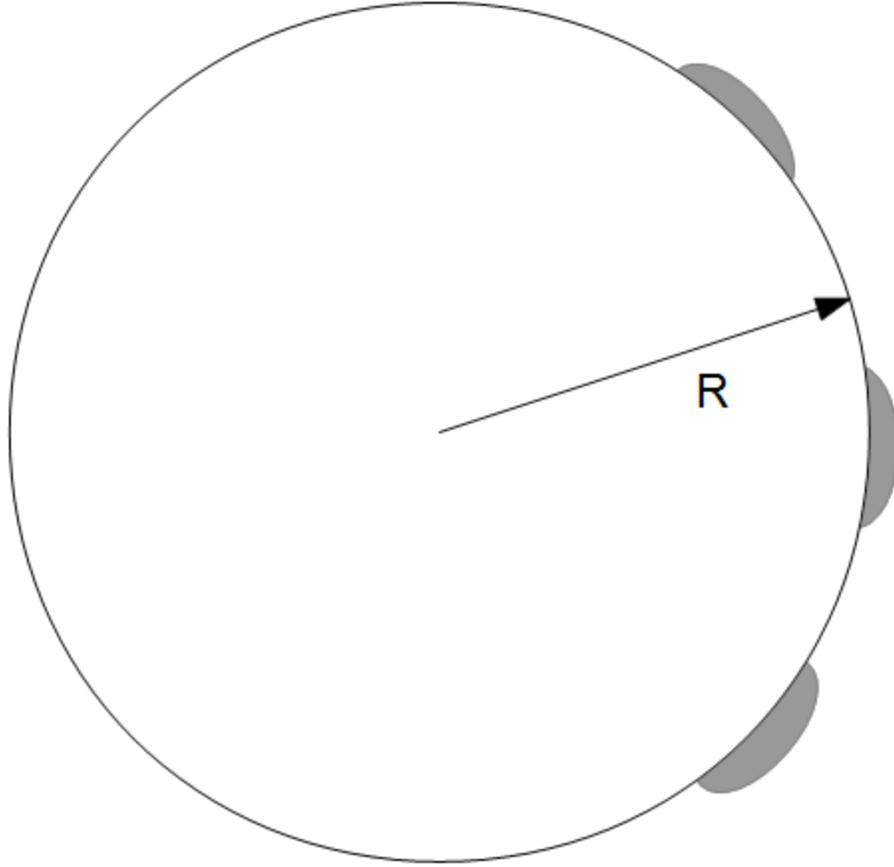


Figure 2. Spherical Fuel Grain Crystal system. Intergranular Bubbles are shown in gray.

In addition, the escaped gas atoms have been shown to rejoin the fuel. This re-resolution of gas into bubbles occurs due to the energy imparted by radiation. Due to this re-resolution, the fuel retains a portion of the gas within its material. To model this, Turnbull changed the perfect sink condition of the problem to an imperfect one [8].

$$C(R,t) = \frac{B(t)N(t)}{D(t)} \quad (4)$$

Here, $B(t)$ is the re-resolution rate from intergranular bubbles in m s^{-1} and $N(t)$ is the gas atom area density at the grain boundary in m^{-2} .

Solutions for this set of conditions are difficult, due to the time-dependent values.

Elton and Lassmann were able to find a solution to this diffusion equation by modifying a solution with a time-constant diffusivity and a time-constant gas generation rate [36].

Here, different values of the diffusivity and gas generation rate were used each timestep, and a correction factor calculated from a fictitious timestep was included to increase the accuracy. Forsberg and Massih found a solution for this system by transforming the diffusion equation into an integral equation. First, the problem is rescaled from t to τ_a in m^2 [9]. Making use of

$$\tau_a = \int_0^t D(t_0) dt_0 \quad (5)$$

the problem is written as

$$\frac{\delta C(r, \tau_a)}{\delta t} = \nabla_r^2 C(r, \tau_a) + \beta_e(\tau_a) \quad (6)$$

Here, $\beta_e(\tau_a) = \beta(\tau_a) / D(\tau_a)$ and has units of m^{-5} . The boundary condition is similarly rewritten as

$$C(R, \tau_a) = \frac{h_1(\tau_a) N(\tau_a)}{2} \quad (7)$$

In this boundary condition, h_1 is defined as

$$h_1 = \frac{B(\tau_a)}{D(\tau_a)} \quad (8)$$

and has units of m^{-1} . Forsberg and Massih [10] had shown that for a perfect sink condition, the total number of gas atoms within the fuel grain can be written as the integral of a series of eigenfunctions over τ_a :

$$\int_0^R 4\pi r^2 C(r, \tau_a) dr = \int_0^{\tau_a} K(\tau_a - \tau_{a0}) \beta_e(\tau_{a0}) d\tau_{a0} \quad (9)$$

The kernel, $K(\tau_a - \tau_{a0})$, has units of m^3 and is defined as

$$K(\tau_a) = \frac{8R^3}{\pi} \sum_{n=1}^{\infty} \frac{e^{-n^2\pi^2\tau_a/R^2}}{n^2} \quad (10)$$

The total amount of gas atoms on the grain boundary can be found in terms of the gas generation and granular gas density. Given the assumption that gas either remains in the fuel or within the intergranular bubbles:

$$4\pi R^2 N(\tau_a) = 2 \left(\frac{4\pi R^3}{3} \int_0^{\tau_a} \beta_e(\tau_{a0}) d\tau_{a0} - 4\pi \int r^2 C(r, \tau_a) dr \right) \quad (11)$$

This equality accounts for gas generated from adjacent fuel grains which share the boundaries by doubling the gas generation and granular gas density. The first term within the parenthesis is the amount of gas generated over time, while the other term states the total amount of gas within the grain. Rewriting the diffusion problem in terms of the difference of gas density from the grain boundary

$$C_0(r, \tau_a) = C(r, \tau_a) - C(R, \tau_a) \quad (12)$$

allows for the use of equation (9), since this formulation uses a perfect sink condition.

Thus,

$$\int_0^R 4\pi r^2 C_0(r, \tau_a) dr = \int_0^{\tau_a} K(\tau_a - \tau_{a0}) \left(\beta_e(\tau_{a0}) - \frac{1}{2} \frac{\partial}{\partial \tau_{a0}} [h_1(\tau_{a0}) N(\tau_{a0})] \right) d\tau_{a0} \quad (13)$$

In this equation, the integral of C_0 identifies the difference in the number of gas atoms of the interior of the grain from its boundary. This combines with equation (11) to form the grain boundary gas area density over time:

$$N(\tau_a) = 2 \int_0^{\tau_a} K_2(\tau_a - \tau_{a0}) \left(\beta_e(\tau_{a0}) - \frac{1}{2} \frac{\partial}{\partial \tau_{a0}} [h_1(\tau_{a0}) N(\tau_{a0})] \right) d\tau_{a0} \quad (14)$$

K_2 is defined as

$$K_2(\tau_a) = \frac{1}{4\pi R^2} \left(\frac{4\pi R^3}{3} - K(\tau_a) \right) \quad (15)$$

The solution is found by taking a Laplace transform in time of equation (14). This transform will replace the rescaled time τ_a to the term s .

$$\bar{N}(s) = \int_0^{\infty} e^{-st} N(\tau_a) d\tau_a \quad (16)$$

The term s has units of s^{-1} . Assuming β_e and h_1 are constants allows

$$\bar{N} = \frac{2\beta_e \bar{K}_2}{s(1 + s\bar{K}_2 h_1)} \quad (17)$$

where \bar{K}_2 is the Laplace transform of equation (15):

$$\bar{K}_2 = R^3 \left(\frac{\coth(R^2 s)^{1/2}}{(R^2 s)^{3/2}} - \frac{1}{(R^2 s)^2} \right) \quad (18)$$

This formulation can be simplified for long and short periods of time. In cases where s is large due to short timespans of t , the $\coth(R^2 s)^{1/2}$ term reduces to 1, so \bar{K}_2 is simplified to

$$\bar{K}_2 = s^{-3/2} - R^{-1} s^{-2} \quad (19)$$

This leads to

$$N(\tau_a) = 2 \frac{\beta_e}{h_1} \left(\tau_a + \frac{1}{h_2 h_3} - \frac{h_2 e^{h_3^2 \tau_a} \operatorname{erfc}(h_3 \tau_a^{1/2}) + h_3 e^{h_2^2 \tau_a} \operatorname{erfc}(-h_2 \tau_a^{1/2})}{h_2 h_3 (h_2 + h_3)} \right) + O(\tau_a^\infty) \quad (20)$$

$$h_2 = -\frac{h_1}{2} + \left(\frac{h_1^2}{4} + \frac{h_1}{R} \right)^{1/2} \quad (21)$$

$$h_3 = \frac{h_1}{2} + \left(\frac{h_1^2}{4} + \frac{h_1}{R} \right)^{1/2} \quad (22)$$

$$\operatorname{erfc}(y) = \frac{2}{\sqrt{\pi}} \int_y^{\infty} e^{-x^2} dx \quad (23)$$

In cases of longer times, the small s allows \bar{K}_2 to simplify to

$$\bar{K}_2 = \frac{R}{3s} - \frac{R^3}{45} + O(s) \quad (24)$$

which integrates to

$$N(\tau_a) = \frac{2\beta_e R}{(3+h_1 R)} \left(\tau_a - \frac{R^2}{5(3+h_1 R)} \right) + \sum_{m=1}^{\infty} \frac{4\beta_e R^3 e^{-(\mu_m/R)^2 \tau_a}}{\mu_m^2 [\mu_m^2 + R h_1 (3 + R h_1)]} \quad (25)$$

with μ_m defined as

$$\mu_m = \arctan\left(\frac{R h_1 \mu_m}{\mu_m^2 + R h_1}\right) + m\pi \quad (26)$$

Due to the heating caused by the fission process, the grains of fuel restructure and grow over time. The change in grain size can relocate the fission gases much more quickly than diffusion, so the diffusion of gas should be reformulated to include the sweeping of gas atoms. Figure 3 shows a representation of the changing spherical system. Forsberg and Massih rescaled the diffusion equation from r to ρ , the dimensionless ratio of r and R [6]. The equation is also rescaled from t to the dimensionless τ .

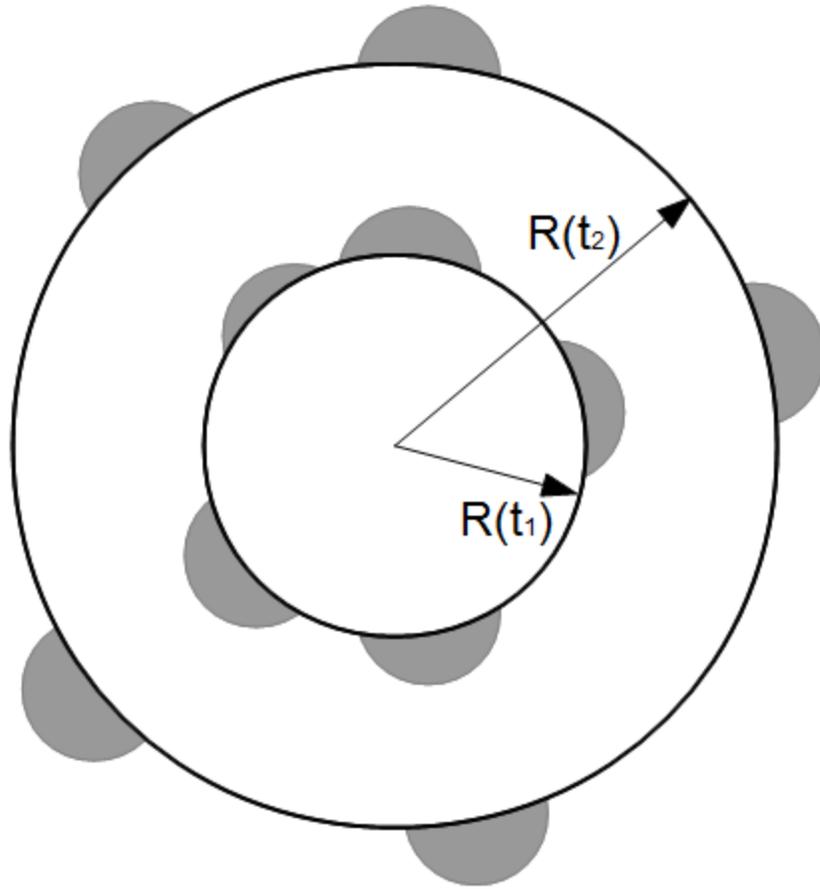


Figure 3. Spherical Fuel Grain Crystal undergoing Crystal Growth. Intergranular Bubbles are shown in gray.

The diffusion equation is shown as

$$\frac{\partial C(\rho, \tau)}{\partial \tau} = \nabla_{\rho}^2 C(\rho, \tau) + P(\tau) \quad (27)$$

where

$$\nabla_{\rho}^2 = \frac{\partial^2}{\partial \tau^2} + \frac{2}{\rho} \frac{\partial}{\partial \rho} + \frac{\partial(\ln R)}{\partial \tau} \rho \frac{\partial}{\partial \rho} \quad (28)$$

$$P(\tau) = \frac{R^2}{D(t)} \beta(t) \quad (29)$$

$$\tau = \int_0^t \frac{D(s)}{R^2(s)} ds \quad (30)$$

The diffusivity D is removed from the diffusion term in equation (27) by placing it in the definition of τ . $P(\tau)$ is the rescaled gas density generation rate, which has units of m^{-3} . Additionally, solution of the above uses the total amount of gas in the crystal. This includes both the gas within the fuel grain and the gas that covers its surface. Before gas escapes the fuel, the grain boundary density of gas can be written as

$$4\pi R^2 N(t) = 2 \left(4\pi \frac{R^3}{3} \int_0^t \beta(v) dv - \int_0^R 4\pi r^2 C(r, t) dr \right) \quad (31)$$

When the imperfect sink boundary condition from equation (4) is used, the total density of gas within and on the grain, $G(t)$, is

$$G(t) = \frac{3D(t)C(R, t)}{2RB(t)} + \frac{3 \int_0^R r^2 C(r, t) dr}{R^3} \quad (32)$$

The first term in the right hand side represents the effects of gas atom re-solution, while the other term is the average gas density of the grain. Rescaling by τ allows for use with equation (27), which forms

$$G(\tau) = \frac{3D(\tau)C(R, \tau)}{2R(\tau)B(\tau)} + 3 \int_0^1 x^2 C(xR, \tau) dx \quad (33)$$

Solution of equation (27) requires separation into particular and complementary solutions.

$$C(\rho, \tau) = C_c(\rho, \tau) + C_p(\rho, \tau) \quad (34)$$

The complementary solution first expands into a sum of basis vectors, separates the time dependence from the answer, and is further estimated as a sum of other vectors.

$$C_c(\rho, \tau) = \sum_{i=1}^{\infty} \alpha_i e^{(-\omega_i \tau)} \sum_{k=0}^{\infty} \lambda_{ik} \tilde{e}_i \quad (35)$$

Here, α_i are the basis vector constants, $e^{(-\omega_i \tau)}$ are the ansatz of the principal time dependence of the solution, and λ_{ik} are the coefficients of the expansion vectors \tilde{e}_i . This assumes that $\lambda_{i0} = 1$, that ω_i causes τ to satisfy the conditions of the problem, and that all \tilde{e}_i satisfy the diffusion and total gas amount equations. This allows \tilde{e}_i to be expressed as

$$\tilde{e}_i = \sum_{m=0}^k \left(\frac{k!}{m!(k-m)!} \right) (2\tau)^{k-m} \binom{m}{i} f \quad (36)$$

where f satisfies

$$\nabla_\rho^2 \binom{m}{i} f + \omega_i \binom{m}{i} f = (2m) \binom{m}{i} f \quad (37)$$

The particular solution of the diffusion equation requires expansion as a power series:

$$C_p(\rho, \tau) = A(\tau) + \sum_{i=1}^{\infty} \zeta_i n_i(\rho, \tau) \quad (38)$$

where

$$A(\tau) = \int_0^\tau P(s) ds \quad (39)$$

The n_i functions satisfy

$$\frac{\partial n_k}{\partial \tau} = \nabla_r^2 n_k \quad (40)$$

$$n_k(r, \tau = 0) = r^{2k} \quad (41)$$

As the intergranular bubble gas density rises, the nuclear fuel undergoes swelling. Unlike swelling from solid fission products and intragranular bubbles, swelling from the ellipsoidal intergranular bubbles ceases once the gas density reaches saturation at N_s . The

swelling can be written as

$$\frac{\Delta V}{V} = \frac{4\pi r_b^3 \omega_\theta}{3} n_b \quad (42)$$

where $\Delta V / V$ is the change in volume of the fuel due to gaseous swelling, r_b is the intergranular bubble radius in units of m, n_b is the intergranular gas bubble density in m^{-3} , and ω_θ is a geometric factor that corrects the error introduced from use of spherical bubbles. It is given as $\omega_\theta = 1 - 1.5 \cos(\theta) + 0.5 \cos^3(\theta)$, where θ is the intergranular bubble dihedral angle. The gas bubble density is assumed to be constant [4], and it is represented in Figure 4.

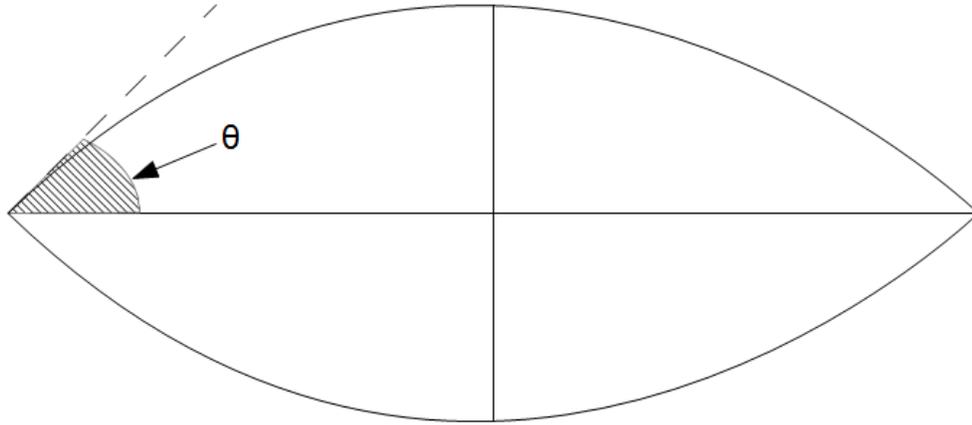


Figure 4. Dihedral Angle of Lenticular Intergranular Bubbles. The angle is used to correct the spherical bubble approximation.

Assuming that the bubble follows the van der Waals Law of gases, the amount of gas atoms in each bubble can be found as

$$N_{atom} = \frac{1}{k_b T} (V_b - bN_{atom}) \left(P + \frac{aN_{atom}^2}{V_b^2} \right) \quad (43)$$

where P is the bubble pressure, T is the temperature, and N_{atom} is the number of gas atoms. In addition, the constants a and b are the van der Waals constants for Xenon, and k_b is the Boltzmann constant. For this method, the aN^2 term is assumed negligible for the gas and removed. The pressure of the gas is shown by Rowlinson and Widom [11] to be

$$P = \frac{2\gamma}{r_b} + P_{\text{ext}} \quad (44)$$

where P_{ext} is the external pressure and γ is the bubble surface tension.

Given that the intergranular gas atom density is $C(R,t) = C_b = N_{\text{atom}} \cdot n_b$, and assuming that equation (44) replaces the pressure term in equation (43), this allows

$$C_b = \frac{4\pi}{3} r_b^3 \omega_\theta n_b \frac{P_{\text{ext}} + 2\gamma / r_b}{b(P_{\text{ext}} + 2\gamma / r_b) + k_b T} \quad (45)$$

By comparing the value of C_b to the intergranular gas atom saturation density of C_{bs} , r_b can be expressed by determining the ratio of r_b and its saturation radius, r_{bs} , as shown in

$$\frac{C_b(t)}{C_{bs}} = x^2 \frac{x + \kappa}{1 + \kappa} \frac{1 + (1 + \kappa)v_p}{1 + (1 + \kappa/x)v_p} \quad (46)$$

where x is the ratio of the current to saturated bubble radii, and κ is the ratio of bubble surface tension to exterior pressure.

$$x = \frac{r_b}{r_{bs}} \quad (47)$$

$$\kappa = \frac{2\gamma}{r_{bs} P_{\text{ext}}} \quad (48)$$

$$v_p = \frac{bP_{\text{ext}}}{k_b T} \quad (49)$$

Once r_b has been determined, equations (40) and (43) may be combined to determine the

swelling

$$\frac{\Delta V}{V} = \frac{3k_b T [1 + (1 + \kappa/x)v_p] N_b}{2P_{ext} (1 + \kappa/x) R} \quad (50)$$

where

$$N_b = \left(\frac{2}{3}\right) RC_b \quad (51)$$

Gas release occurs from two different modes: from diffusion out of the grain and from grain boundary sweeping. Since one of these two modes tends to dominate, one of these modes may be simplified by removing it from consideration. The dominant mode can be determined by comparing D/R^2 and $(dR/dt)/R$. Situations where D/R^2 greatly exceed $(dR/dt)/R$ simplify to the static grain radius model. In those cases, the problem should be solved using only that model. For problems where $(dR/dt)/R$ greatly exceed D/R^2 , gas release is derived from equation (32). It is found by deriving the change in the average gas density in the grain from the second term while using equation (4) in place of $C(R,t)$. This creates

$$\frac{d\bar{C}(t)}{dt} = \frac{3}{R} \left(\frac{B}{D} N - \bar{C}(t) \right) + \beta(t) \quad (52)$$

where $\bar{C}(t)$ is the average gas density within the grain. This value allows for the solution of the fractional gas release

$$\tilde{F} = 1 - \tilde{C} \quad (53)$$

where \tilde{F} is the fractional release and

$$\tilde{C} = \frac{\bar{C}(t)}{\int_0^t \beta(v) dv} \quad (54)$$

Before release, all gas is considered to be within the grain boundary and interior, so for all times before gas release

$$\bar{C}(t) = \int \beta(t) dv \quad (55)$$

In addition, there are two schemes of modeling fission gas release: discrete release and continuous release. In discrete release, a fraction of the gas in the interconnected bubble network escapes the fuel once the bubbles reach saturation value. The remaining fraction waits in the bubbles until it reaches the saturation density again. The continuous release scheme assumes that the cycle of accumulation and release occurs multiple times within a given timestep. Modeling the release from this scheme requires an average density of gas, which is determined by the largest and smallest densities for the release cycle. For this model, all the gas is assumed to escape the fuel during continuous release, so the effective gas surface area density in equation (55) is half the saturation value.

CHAPTER 3

METHODOLOGY

The volume swelling is calculated from equation (42) and utilizes equations (43), (45), and (46). As $C_{bs} = (3/2)(N_{bs}/R)$, N_{bs} is determined as

$$N_{bs} = \frac{4r_{bs}\omega_{\theta}f_b P_{ext}(1+\kappa)}{3k_b T \sin^2 \theta [1 + \nu_p(1+\kappa)]} \quad (56)$$

where f_b is the fractional coverage of bubbles over grain surfaces. In their 1985 paper, Forsberg and Massih assumed a constant grain radius to determine the gas surface area density [9]. Replacement with the model created in their 2007 paper allows for modeling of the gas release and the swelling as the fuel reshapes [6]. These methods can be used by limiting the infinite series in equation (35) to

$$C_c(\rho, \tau) = \sum_{i=1}^3 \alpha_i e^{(-\omega_i \tau)} \sum_{k=0}^2 \lambda_{k,i} \tilde{e}_i \quad (57)$$

as well as limiting the last term i in the sum in equation (38) to 2. These approximations enable MATLAB to run a script that numerically solves these equations, and the equations are written as

$$C(\rho, \tau) = e(\rho, \tau) = e_0 + \sum_{i=1}^3 \alpha_i e_i(\rho, \tau) \quad (58)$$

For this equation, e_0 is the particular solution, and the sum of e_i is the complementary solution. The intergranular gas density $C(\rho = 1, \tau) = C_b$ is determined by finding both the complementary and particular solutions. First, for the complementary solution, the terms ${}^m_i f$ in equation (36) are solved from equation (37). The solution takes the form of spherical Bessel functions of the first kind.

$${}_i^m f = (\mu_i R)^{-2m} (\mu_i r)^m j_m(\mu_i r) \quad (59)$$

In this equation, j_m is the Spherical Bessel function, and $\mu_i R = (\omega_i)^{1/2}$ [37]. These functions are solutions to the Helmholtz equation in spherical coordinates.

$$x^2 \frac{\partial^2 w}{\partial x^2} + 2x \frac{\partial w}{\partial x} + (x^2 - m(m+1))w = 0 \quad (60)$$

Here, x is the independent variable, w is the dependent variable, and m is the order of the Bessel function. Spherical Bessel functions are defined in terms of cylindrical Bessel functions J_m , as shown below.

$$j_m(x) = \sqrt{\frac{\pi}{2x}} J_{m+1/2}(x) \quad (61)$$

The cylindrical Bessel functions are defined as follows:

$$J_m(x) = \sum_{n=0}^{\infty} \frac{(-1)^n}{n! \Gamma(m+n+1)} \left(\frac{x}{2}\right)^{2m+n} \quad (62)$$

$$\Gamma(n) = \int_0^{\infty} x^{n-1} e^{-x} dx \quad (63)$$

$\mu_i R$ are determined for values of i up to 3 at two different times. In the case of discrete gas release, the values are determined by the integral equation condition in equation (33) for the functions ${}_0 \tilde{e}_i$ instead of the density C . For values of i greater than 0, the equation transforms into

$$0 = \frac{D(\tau) {}_0 \tilde{e}_i(R, \tau)}{2R(\tau) B(\tau)} + \int_0^1 x^2 {}_0 \tilde{e}_i(xR, \tau) dx \quad (64)$$

Since ${}_0 \tilde{e}_i(r, \tau) = j_0(\mu_i r)$, the solution for $\mu_i R$ is found by integration of equation (64).

$$\mu_i R = \arctan \left(\frac{\mu_i R}{(\mu_i R)^2 \frac{D}{(2BR)} + 1} \right) + i\pi \quad (65)$$

As this is a transcendental equation, a numerical solution is necessary.

In the case of continuous gas release, the complementary solution satisfies the boundary equation

$$e_i(\rho, \tau) = 0 \quad (66)$$

for all nonzero i . Thus, determination of $\mu_i R$ is performed by setting ${}_0\tilde{e}_i = 0$. This leads to the solution shown below.

$$\mu_i R = i\pi \quad (67)$$

Next, ${}_0e_i$, ${}_1e_i$, and ${}_2e_i$ are found from each $\mu_i R$. Given that ${}_i\lambda_0 = 1$ and that ${}_i\lambda_k$ are constant over the run time of the script, and utilizing the following:

$$\sum_{k=0}^2 {}_i\lambda_k {}_k e_i(\rho = 1, \tau) = 0 \quad (68)$$

${}_i\lambda_1$ and ${}_i\lambda_2$ can be found by setting a system of equations.

For the particular solution, the conditions of equation (38) are rewritten as

$$C_p(\rho, \tau) = e_0(\rho, \tau) \approx \sum_{k=0}^2 A_k(\tau) {}_k e_0(\rho, \tau) \quad (69)$$

$$\xi_0 = A_0 = \int_0^\tau P(s) ds \quad (70)$$

where ${}_k e_0$ all satisfy the following conditions.

$$\frac{\partial}{{\partial\tau}} {}_k e_0 = \nabla_{\rho}^2 {}_k e_0(\rho, \tau) \quad (71)$$

$${}_k e_0(\rho, \tau = 0) = \rho^{2k} \quad (72)$$

The solution of ${}_k e_0$ for these conditions is a power series expansion of

$${}_0 e_0(\rho, \tau) = 1, \quad {}_1 e_0(\rho, \tau) = \rho^2 + 6\tau, \quad {}_2 e_0(\rho, \tau) = \rho^4 + 20\rho^2\tau + 60\tau \quad (73)$$

Λ_1 and Λ_2 are determined by setting a system of equations similar to equation (68) for

$$\sum_{k=0}^2 A_k \tilde{e}_0(\rho = 1, \tau) = 0 \quad (74)$$

The values of α_i are determined [12] from the equation

$$w_m = \sum_{i=1}^3 A_i M_{mi}(R_0) + \sum_{i=1}^3 \left(\sum_{k=0}^2 \lambda_k (\mu_i R_0)^k M_{mki}(R_0) \right) \cdot \alpha_i \quad (75)$$

where w_m is the generalized moment of the particular and complementary solutions, and

where

$$M_{mi}(R_0) = R_0^{2i} \int_0^1 x^{2i+2} j_0(m\pi x) dx \quad (76)$$

$$M_{mki}(R_0) = \int_0^1 x^{k+2} j_0(m\pi x) j_k(\mu_i R_0 x) dx \quad (77)$$

The generalized moment is given by

$$w_m[R(\tau)] = \frac{1}{R(\tau)} \int_0^{R(\tau)} \rho^2 j_0\left(\frac{m\pi x}{R(\tau)}\right) e(\rho, \tau) d\rho \quad (78)$$

and its values for the complementary and particular solutions are given in Appendix A.

When equation (75) is rewritten in the form of

$$\sum_{i=1}^3 A_{im} \alpha_i = \beta_m \quad (79)$$

then it allows for solution by means of matrix division

$$\alpha = A_v^{-1} \beta_v \quad (80)$$

Here, A_v is the matrix form of A_{im} , β_v is the vector form of β_m , and A_{im} and β_m are the

rearranged terms of equation (75).

$$A_{i_m} = \sum_{k=0}^2 \lambda_k (\mu_i R_0)^{-k} M_{mki}(R_0) \quad (81)$$

$$\beta_m = w_m - \sum_{i=1}^3 A_i M_{mi}(R_0) \quad (82)$$

With all the values listed, the grain boundary gas density C_b is defined as

$$C_b = \sum_{k=0}^2 A_{k k} \tilde{e}_0(R, \tau) + \sum_{i=1}^3 \alpha_i e^{-\omega_i \tau} \sum_{k=0}^2 \lambda_{k k} \tilde{e}_i(R, \tau) \quad (83)$$

Once C_b is found, equation (46) may be used in the form of

$$\frac{x^3(x+\kappa)}{x+(x+\kappa)v} = \frac{1+\kappa}{1+(1+\kappa)v} \frac{C_b}{C_{bs}} \quad (84)$$

Solving this transcendental equation for x allows equation (50) to yield the volumetric swelling over time.

Gas release is determined in the case where $(dR/dt)/R$ exceeds D/R^2 . First, the value of equation (52) is determined for a given time. This value is multiplied by the simulation timestep and added to $\overline{C}(t)$. Then, $\overline{C}(t)$ is divided by the total density of generated gas. This determines \tilde{C} , which allows for solution of the fractional and total gas release.

Forsberg and Massih designed these models of diffusion, swelling, and gas release from the properties of UO_2 . The models they constructed require input parameters for the diffusion of gas through fuel and the growth of fuel grains. Fission gas diffusion for UO_2 is given in the form of

$$D = \frac{D' v_g}{v_g + g} \quad (85)$$

where v_g and other parameters are given in given in Table 1. The fission density and other properties of UO_2 are given in Table 2. Both tables are assembled from the combined research of Speight, Turnbull et al, White and Tucker, and Matzke [13] [14] [15] [16].

The diffusivity of UO_2 in a trap-free medium in Table 1 is given as three terms: a high temperature thermal term taken from Davis and Long [38], and two irradiation terms taken from Turnbull [14]. The combined thermal and irradiation term relates to the irradiation induced cation vacancies in the fuel, while the third term does not have a set mechanism. The trap-like nature of intragranular bubbles reduces the effective diffusivity of the nuclear fuel. This diffusivity is determined from intragranular gas bubble re-resolution rate, v_g , and the fission gas capture rate from intragranular bubbles, g . Given the fission density and temperature range simulated, these competing interactions reduced the effective gas diffusivity by an order of magnitude.

The fission gas production rate, β , appears in equation (121) of White's 1983 [15] paper. This production rate was originally created by Schilling [39], and the rate used by Forsberg and Massih appears to be a simplification for fission densities on the order of $10^{19} \text{ m}^{-3} \text{ s}^{-1}$.

The formulation of grain growth chosen from this model originates from Jernkvist's and Massih's [17] work, and is given in the form of

$$\frac{dR}{dt} = \frac{k_g}{2} \left(\frac{1}{2R} - \frac{1}{D_{m,UO_2}} \right) \quad (86)$$

$$D_{m,UO_2} = D_0 \left[H(T_g - T) + H(T - T_g) A_m e^{-Q_m/T} \right] \quad (87)$$

$$k_{g,UO_2} = A_g e^{-Q_g/T} \quad (88)$$

Here, D_{m,UO_2} is the maximum grain diameter, D_0 is the initial grain diameter, T_g is 1550 K, A_m is 615.59, Q_m is 9955 K, A_g is $4.11 \times 10^{-9} \text{ m s}^{-1}$, and Q_g is 32114.51 K. The H function shown here is the Heaviside step function. This function is used to restrict grain growth to temperatures above 1550 K, since $H(x) = 0$ for all x less than zero. Values of x greater than zero cause $H(x) = 1$. The formula for grain growth is taken from the model used by Turnbull [40].

Table 1. UO₂ gas diffusion parameters. Values are taken from [13], [14], [15], and [16].

$D' = C_1 e^{-Q_1/(k_b T)} + C_2 \dot{F} e^{-Q_2/(k_b T)} + C_3 \dot{F}$	m ² s ⁻¹	Diffusivity in trap-free media
$v_g = 3.03\pi l \dot{F} (\bar{R}_b + \delta)^2$	s ⁻¹	Intragranular gas bubble resolution rate
$\bar{R}_b = 1.453 \times 10^{-10} \cdot e^{1.023 \times 10^{-3} T}$	m	Intragranular bubble radius
$g = 4\pi \bar{R}_b C_b' D'$	s ⁻¹	Fission gas capture rate by intragranular gas bubbles
$C_b' = 1.52 \times 10^{27} / T - 3.3 \times 10^{23}$	m ⁻³	Total bubble density
$l = 6 \cdot 10^{-6}$	m	Fission fragment range
$\delta = 10^{-9}$	m	Damage radius of fission fragment
$\dot{F} = N_a \dot{F}_m$	m ⁻³ s ⁻¹	Fission density
$\dot{F}_m = 5.189 \times 10^{-14} q_v$	mol m ⁻³ s ⁻¹	Molar fission density
q_v	W m ⁻³	Power density
$\beta = 0.3 \dot{F}_m$	mol m ⁻³ s ⁻¹	Molar fission gas production rate
$N_a = 6.022 \times 10^{23}$	mol ⁻¹	Avogadro constant
$Q_1/k_b = 35247$	K	Activation energy / k _b
$Q_2/k_b = 13800$	K	Activation energy / k _b
$C_1 = 7.6 \times 10^{-10}$	-	-
$C_2 = 4.5 \times 10^{-35}$	-	-
$C_3 = 2.0 \times 10^{-40}$	-	-

Table 2. Fuel power density and other input parameters of UO₂. Values are taken from [13], [14], [15], and [16].

$d_{pellet} = 9.00$	mm	Fuel pellet diameter
$\rho_T = 0.950$	-	Fraction of fuel density
$D_O = 10$	μm	Initial fuel grain size
$P_{ext} = 100,000$	Pa	External pressure
$\frac{4r_{bs}\omega_{\theta}f_b}{3\sin^2\theta} = 7.25 \times 10^{-8}$	m	Composite gas bubble parameter
$\frac{2B(t)}{\beta(t)} = 5.7 \times 10^{-8}$	$\text{m}^4 \text{mol}^{-1}$	Ratio of re-resolution rate to gas production rate
$b = 5.16 \times 10^{-5}$	$\text{m}^3 \text{mol}^{-1}$	van der Waals constant for Xenon
$q_l = 35$	kW m^{-1}	Linear power density

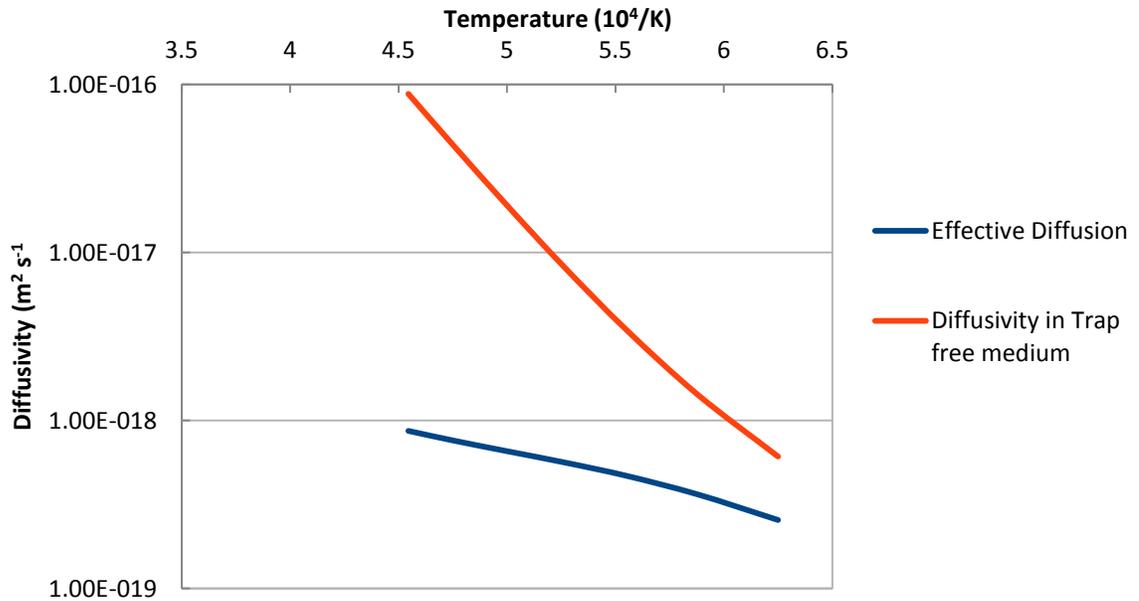


Figure 5. The diffusivity ($\text{m}^2 \text{s}^{-1}$) of UO₂ over inverse temperature ($10^4 / \text{K}^{-1}$).

Nuclear fuel which behaves in a similar fashion to UO_2 may be used in this model as well. Fisher et al report that some MOX fuels act in a similar fashion to UO_2 [18]. In these fuels, the intergranular bubble network is disrupted by areas of concentrated Pu. Fuels with maximum diameter areas of $200 \mu\text{m}$ do not form a bubble network in the operation conditions of Pressurized Water Reactors [19]. However, quasi-homogenous SBR fuels form a perturbed network. In this style of fuel, the areas of concentrated Pu have diameters of up to $35 \mu\text{m}$. Fisher et al quantitatively determined that this perturbed network is within the ranges seen in UO_2 [18]. The rate of fission gas generation is comparable [20]. Irradiation re-solution of gas atoms is reported to occur [21]. The diffusion parameter for MOX fuels is currently unstudied, but it is assumed to be the same. This assumption is supported by comparing the release of fission products and stable gases. Uffelen et al [22] found that the composition of the MOX fuel mattered far less for grain growth than the fabrication process. Porosity due to the manufacturing process was shown to be inversely proportional to grain growth rates. They created a set of equations from the work of Nichols [23] that describe the grain growth of MOX as

$$\frac{dR}{dt} = \frac{k_{g,MOX,N}}{64R^3}, \text{ if } 2R < D_m \quad (89)$$

$$\frac{dR}{dt} = 0, \text{ if } 2R > D_m$$

$$k_{g,MOX,N} = 8.7075 \times 10^{-14} \cdot e^{(-46524/T)}, D_{m,MOX,N} = 3.345 \times 10^{-3} \cdot e^{(-7620/T)}$$

Here, k_g is in units of $\text{m}^4 \text{s}^{-1}$. Another equation he uses to describe the growth is given as

$$\frac{dR}{dt} = \frac{k_{g,MOX,S}}{24R^2} \quad (90)$$

$$k_{g,MOX,N} = 4.25 \times 10^{-11} \cdot e^{(-38396/T)}$$

and it is derived from the work of Sari [24]. Here, k_g uses units of $m^3 s^{-1}$. Figures 6 and 7 show the growth of the fuel grains over time.

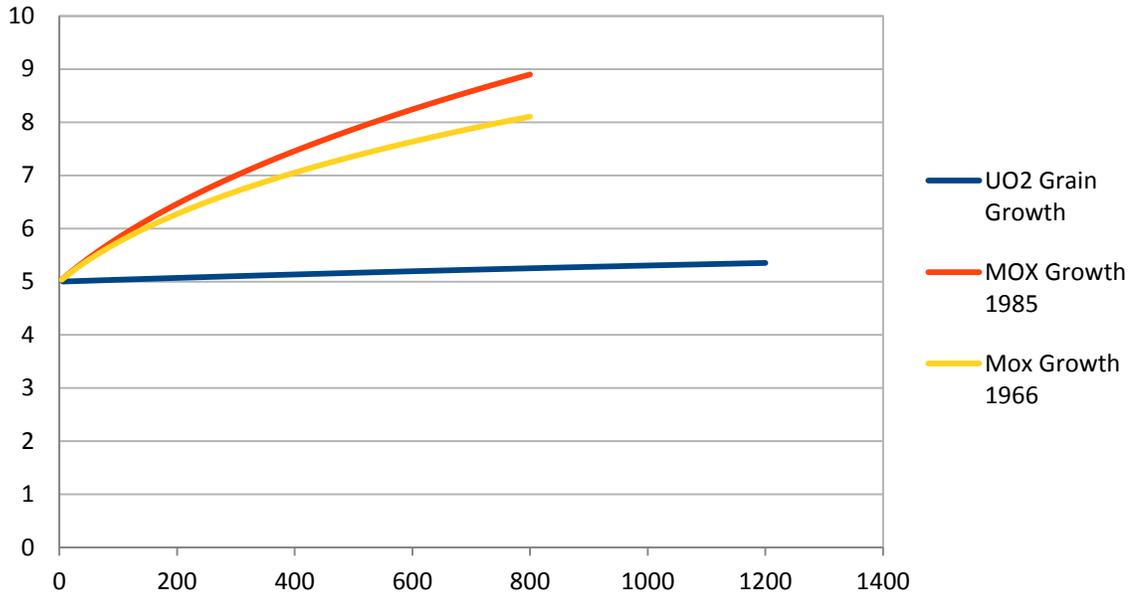


Figure 6. Fuel Grain Size (μm) at 1600 K over Time (hr).

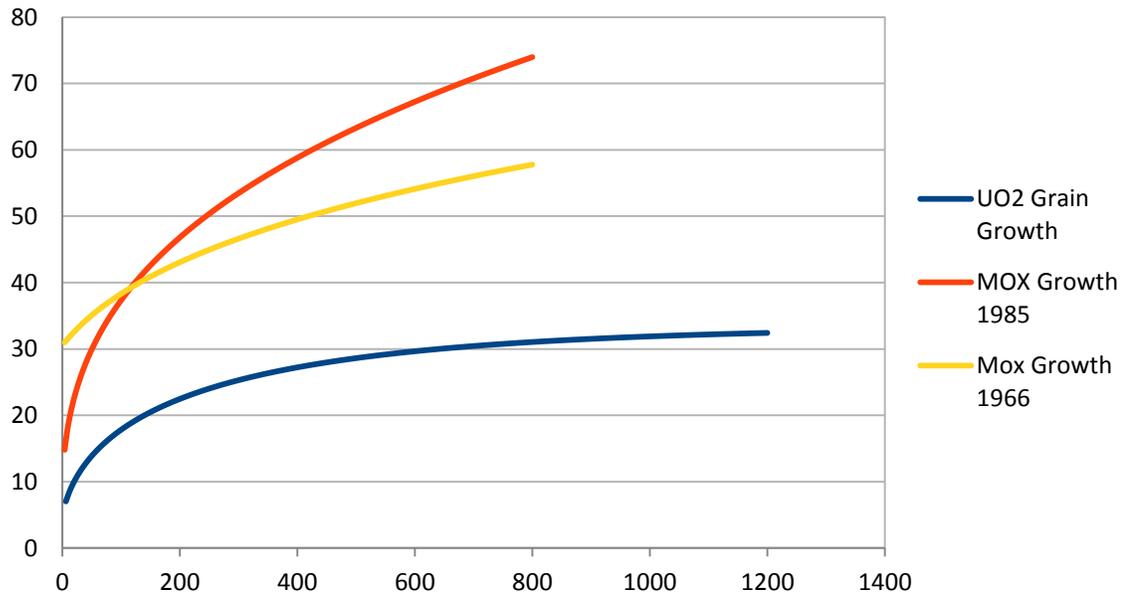


Figure 7. Fuel Grain Size (μm) at 2200 K over Time (hr).

Thorium oxide fuel appears to act as a candidate as well. While it is an understudied fuel, its similarity to UO₂ allows for reasonable approximations to be made of its diffusion parameter [25]. Gas re-solution and release are expected to behave similarly. However, the grain growth rate of ThO₂ has been noted [26] as

$$\frac{dR}{dt} = \frac{k_{g,ThO_2} N}{24R^2} \quad (91)$$

$$k_{g,ThO_2} N = 2.22 \times 10^{-13} \cdot e^{(-435000(8.3144T))} \quad (92)$$

Due to this growth rate, D/R^2 exceeds $(dR/dt)/R$ for conventional grain sizes (5×10^{-6} m). Since diffusion far exceeds gas atom relocation by grain boundary sweeping, ThO₂ should be treated using Forsberg and Massih's static grain radius model.

Some Uranium-based metallic fuels also are fit for this model. U-Pu-Zr in the α phase does not form an intergranular bubble network [27]. It forms a dense cluster of pores. However, the high temperature γ phase allows the network to form [28]. The re-solution of gas atoms from bubbles is well noted [29]. However, grain growth for Uranium alloys in the γ phase is currently unstudied. Without this information, gas release and swelling of metallic fuels cannot be determined.

CHAPTER 4

RESULTS

Benchmark data for the fixed grain radius are shown in Figure 8. The reproduced data is generated from a MATLAB script and compared to Figure 1 from their 2008 paper [5]. For these runs, the grain radius was 7.5×10^{-6} m; all other values are taken from Tables 1 and 2. The slight difference in the 1900 K and 1700 K runs appears to be due to rounding errors from the solution of equation (46).

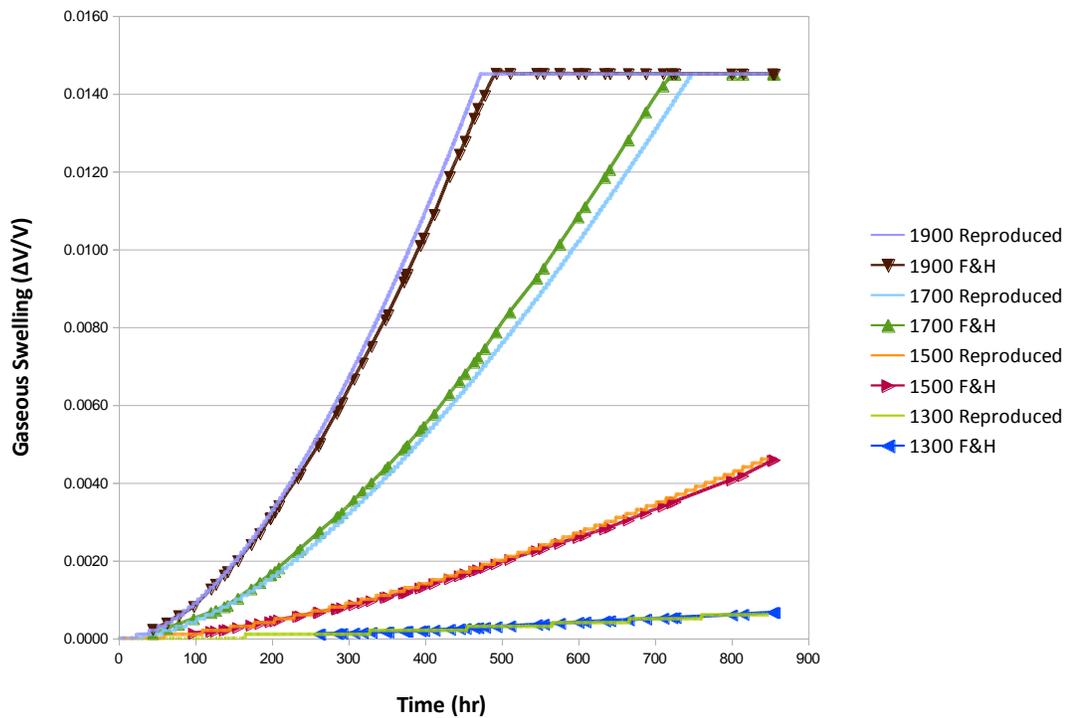


Figure 8. Benchmark of Gaseous Swelling over Time (hr) of Fixed Grain Radius Model with Forsberg and Massih's data [5].

The results of the fixed grain radius model of gas diffusion for temperatures from

1600 to 2200 K are shown below. Figure 9 shows the intergranular gas density over time, while Figure 10 shows the gaseous swelling over time. These simulation runs used the analytical solution presented in [9] for gas diffusion while utilizing the parameters shown in Tables 1 and 2. These runs assume that the gas density and gaseous swelling are constant after reaching saturation. Table 3 shows sample data from the MATLAB script which generated the values. Note that gas release is not calculated with this analytic solution, as no inventory of gas within the grain is kept. Also, SBR MOX fuel is not included in these figures, as it is assumed to share the same gas atom diffusivity.

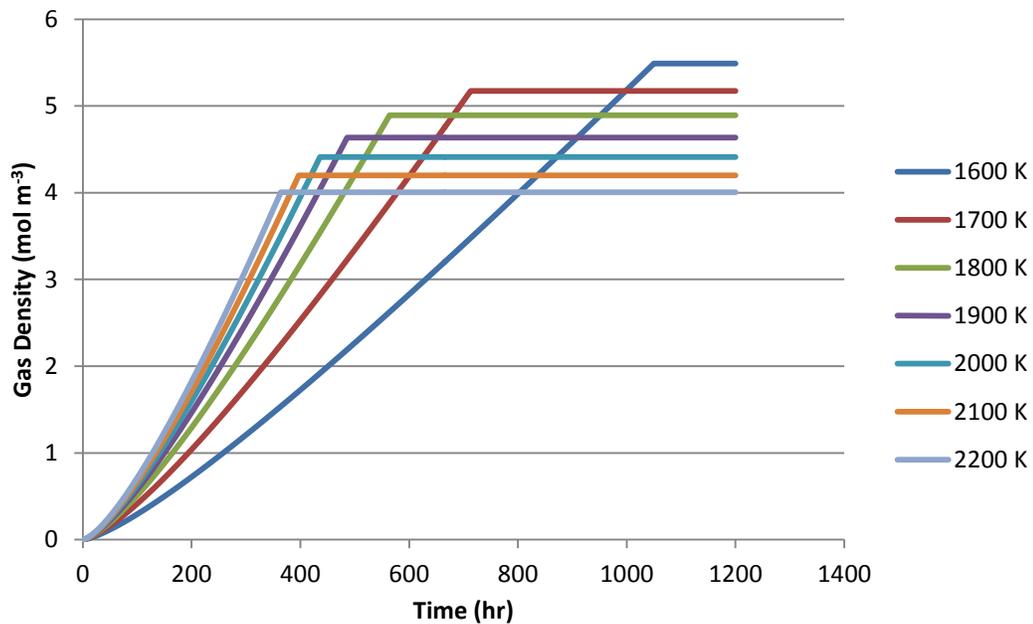


Figure 9. Intergranular gas density (mol m^{-3}) over time (hr) of UO_2 for various temperatures (K) and for a fixed grain radius of $5 \mu\text{m}$.

Table 3. Sample data of Forsberg and Massih's fixed grain radius gas diffusion model for 1900 K.

Time (hr)	$x (r_b/r_{bs})$	Intergranular Gas Volumetric Density (mol m^{-3})	Gaseous Swelling
20	0.14369	0.0602	0.0001
40	0.2294	0.1614	0.0002
60	0.29982	0.2848	0.0005
80	0.36128	0.4243	0.0009
100	0.41655	0.5764	0.0013
120	0.46716	0.7389	0.0018
140	0.51409	0.9102	0.0025
160	0.55801	1.0892	0.0031
180	0.5994	1.2749	0.0039
200	0.63862	1.4667	0.0047

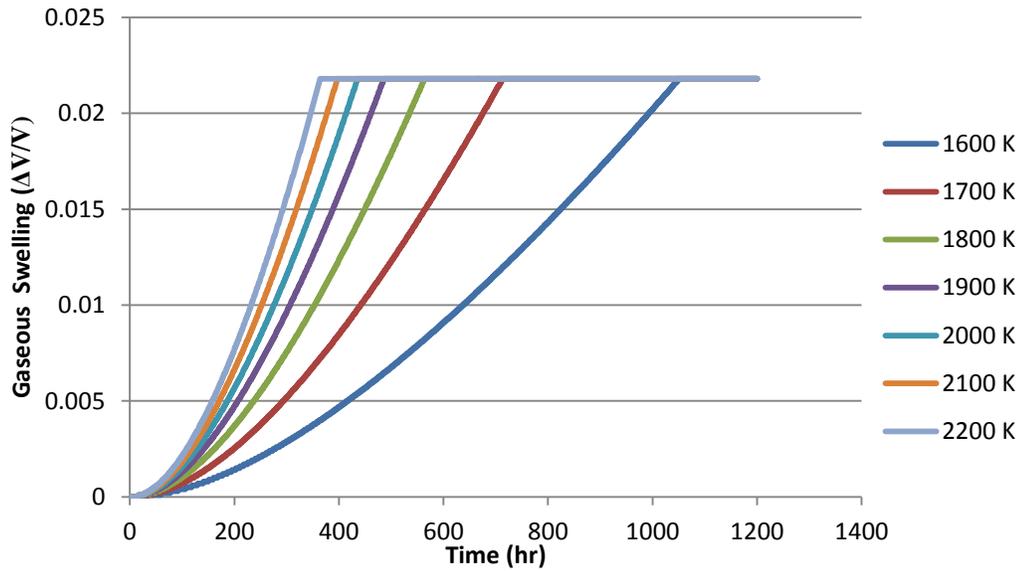


Figure 10. Gaseous Volumetric Swelling of UO_2 over time (hr) for various temperatures (K) at a fixed grain radius of 5×10^{-6} m.

Figure 11 demonstrates the effects of grain radius on the swelling kinetics. The figure shows an inverse relationship between grain radius and both the total swelling and the time needed to reach intergranular saturation. Since the rate of gas generation is related to the amount of mass within the grain, a decreased grain volume and mass would increase the time needed to saturate the surrounding intergranular bubbles. Also, smaller grain volumes increase the total grain boundary area within the fuel, which increases the number of places where intergranular bubbles occur.

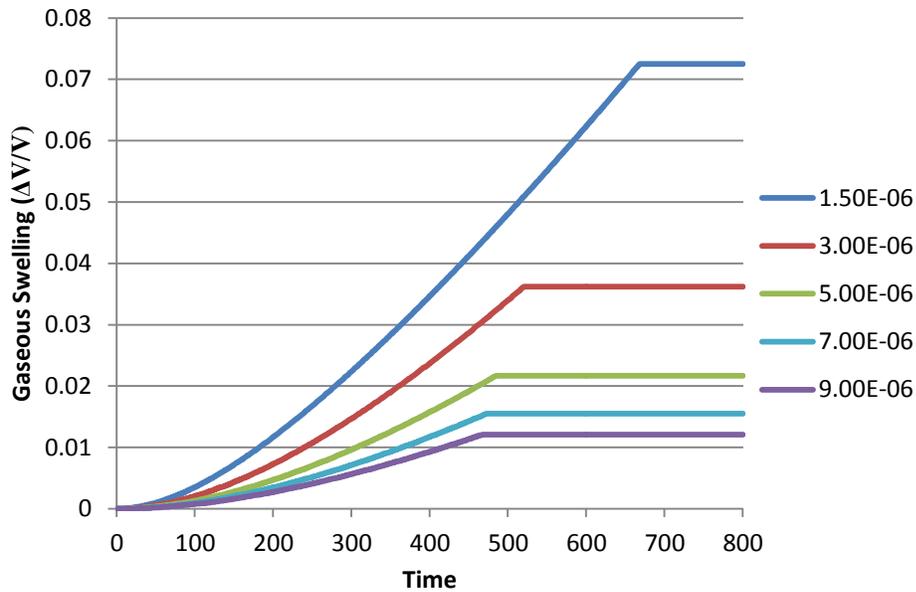


Figure 11. Gaseous Volumetric Swelling of UO_2 over time (hr) for various Grain Radii (m) at a fixed temperature of 1900 K.

Simulations were also run for the numerically solved grain growth models. Temperatures from 1600 K and 2200 K were employed, and the diffusivity coefficient and input parameters of UO_2 were used. The grain growths were from Jernkvist and

Massih for UO_2 and from Nichols and Sari and MOX. Diffusion and fuel parameters were taken from Tables 1 and 2 with the exception of the composite gas bubble parameter. In the MOX fuel simulations, that parameter was recalculated with a bubble dihedral angle of 56° . Gas release was calculated in the continuous scheme, which makes use of equation (66). Sample values generated from the MATLAB script are shown in Table 4. Figure 12 compares some data from UO_2 runs to benchmark data from Forsberg and Massih [6]. The generated data does not conform to the benchmark data for temperatures at 1700 K. The generated data provides a closer match for other temperatures. The reason for the divergence appears to be due to the unstated fission gas release scheme used to generate the benchmark data in their paper.

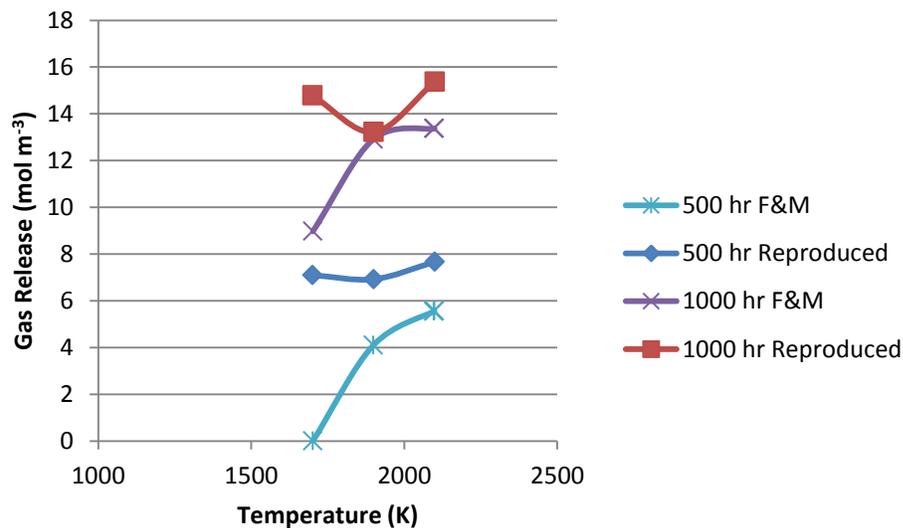


Figure 12. Benchmark of Gaseous Swelling over Time (hr) of Grain Growth Model with Forsberg and Massih's data [6].

Figures 13, 14, and 15 show the intergranular gas density of the three correlations

of grain growth over time. These figures excise gas density data after saturation is achieved. The intergranular gas density reaches its maximum values much more quickly for larger temperatures, but the resulting larger grains reduce the gas volumetric density required for saturation and interlinkage.

Table 4. Sample data of Forsberg and Massih’s grain growth model for 1900 K.

Time (hr)	$x (r_b/r_{bs})$	Fractional Fission Gas Release	Intergranular Gas Volumetric Density (mol m^{-3})	Gaseous Swelling
30	0.14398	0	0.05835	0.000055
60	0.31785	0	0.27885	0.00053
90	0.50854	0	0.70633	0.001988
120	0.70828	0	1.3708	0.005006
150	0.91245	0	2.29272	0.010096
180	1	0.40859	2.69182	0.012647
210	1	0.41994	2.57864	0.012116

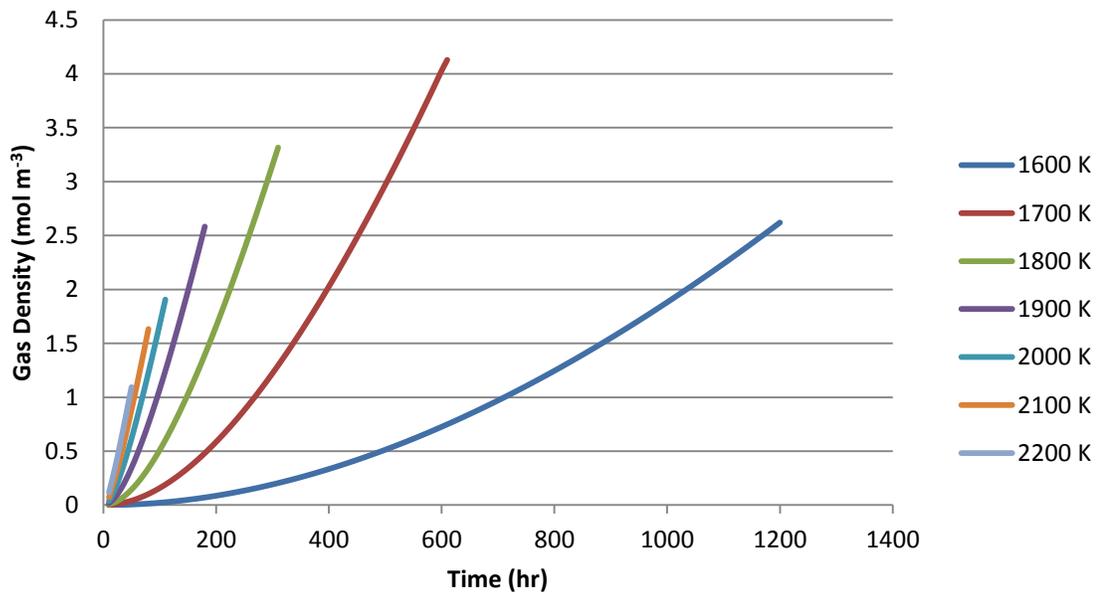


Figure 13. Intergranular gas density (mol m^{-3}) over time (hr) for various temperatures (K) using Jernkvist and Massih’s model of grain growth for UO_2 [17].

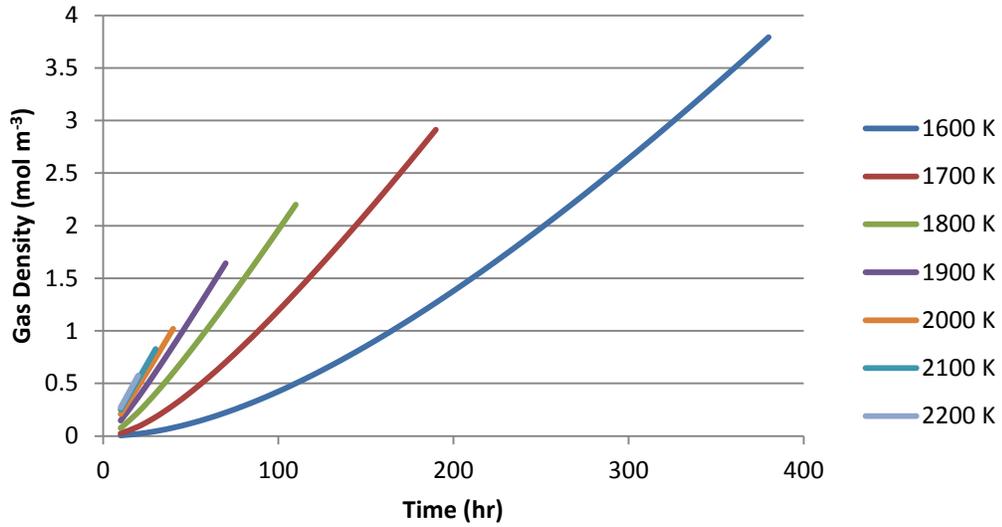


Figure 14. Intergranular gas density (mol m^{-3}) over time (hr) for various temperatures (K) using Nichols' fourth power grain growth equation for hour [23].

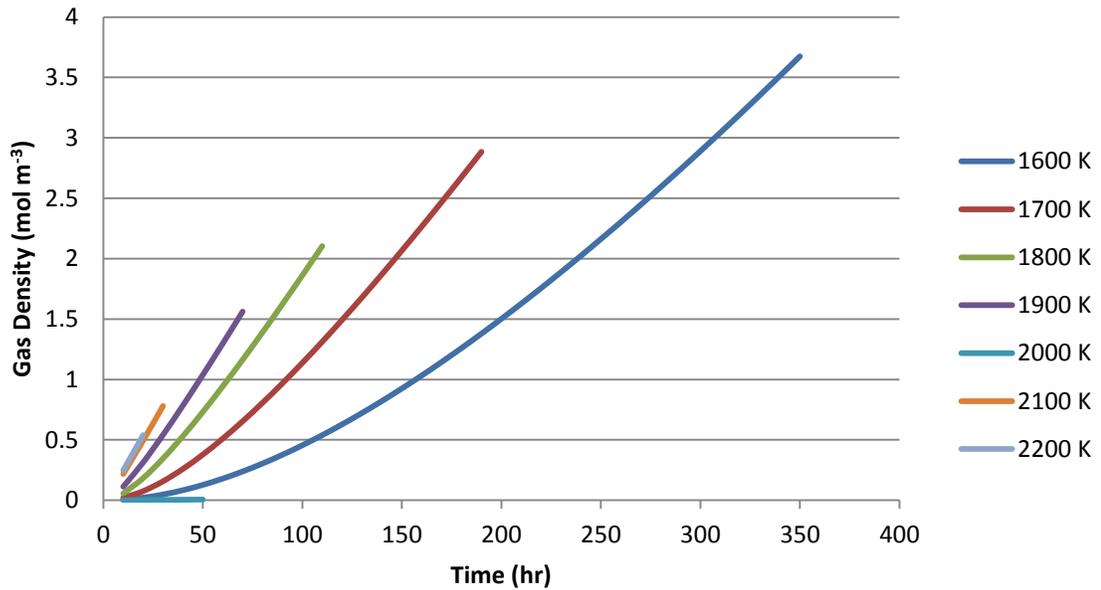


Figure 15. Intergranular gas density (mol m^{-3}) over time (hr) for various temperatures (K) using Sari's cubic grain growth equation for MOX [24].

Figures 16, 17, and 18 show the gaseous fuel swelling over time for the simulated fuels. The swelling here is calculated for an intergranular gas bubble saturation radius of $1\ \mu\text{m}$. As with the intergranular gas density of the fuels, the fuel swelling is greater with lower temperatures, but it requires longer times to achieve the maximum swelling. The swelling peaks and declines as the fuel grains grow and the intergranular gas density shrinks.

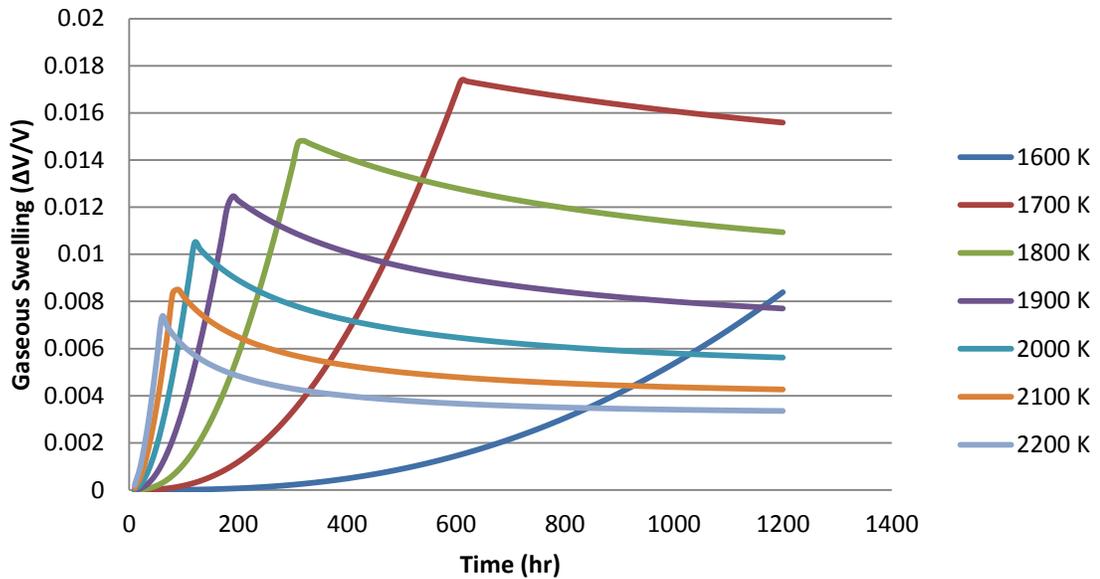


Figure 16. Gaseous Volumetric Swelling over time (hr) for various temperatures (K) using Jernkvist and Massih's model of grain growth for UO_2 [17].

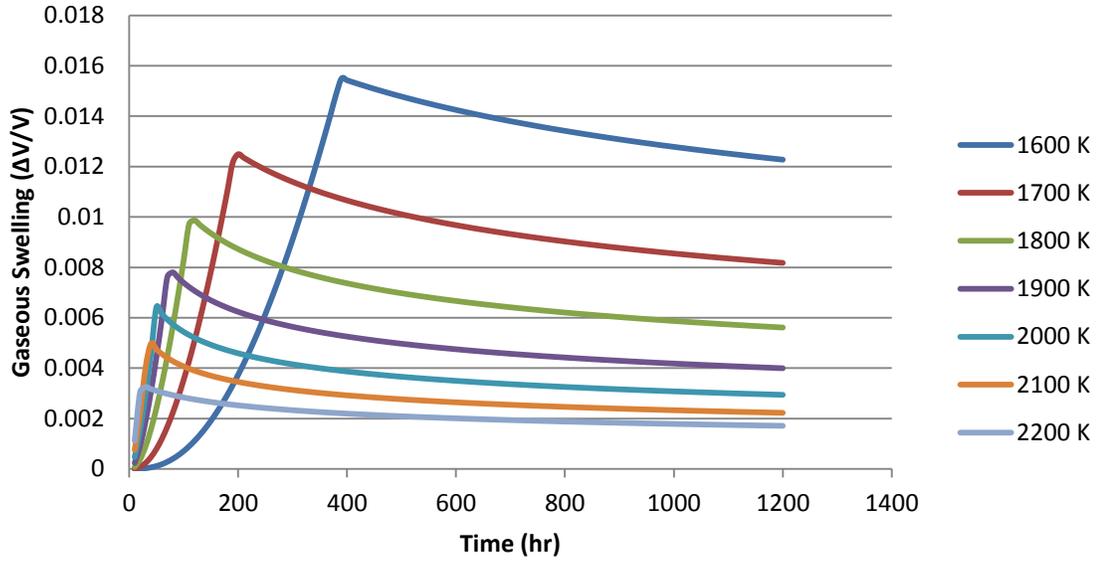


Figure 17. Gaseous Volumetric Swelling over time (hr) for various temperatures (K) using Nichols' fourth power grain growth equation for MOX [23].

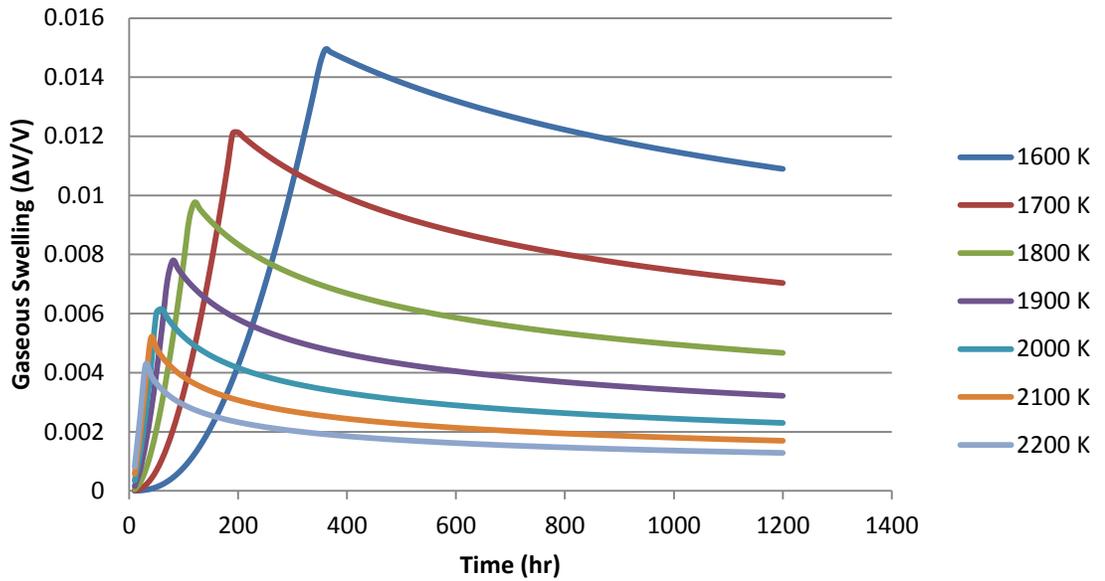


Figure 18. Gaseous Volumetric Swelling over time (hr) for various temperatures (K) using Sari's cubic grain growth equation for MOX [24].

The fractional gas release of UO_2 and SBR MOX for a constant initial grain radius of 5×10^{-6} m is shown in figures 19, 21, and 22. At low temperatures, once the intergranular density reaches saturation and the gas escapes the fuel, the fractional release continues to climb. At intermediate temperatures in UO_2 , the fractional release grows, peaks, and decreases. High temperatures in UO_2 have large initial fractional releases which decrease over time. This behavior is due to both the retarding influence of average granular gas density and the increasing fuel radius in equation (52). The fractional releases in MOX appear to converge to a single temperature-independent value, due to the lack of temperature dependent maximum grain size for the simulation parameters.

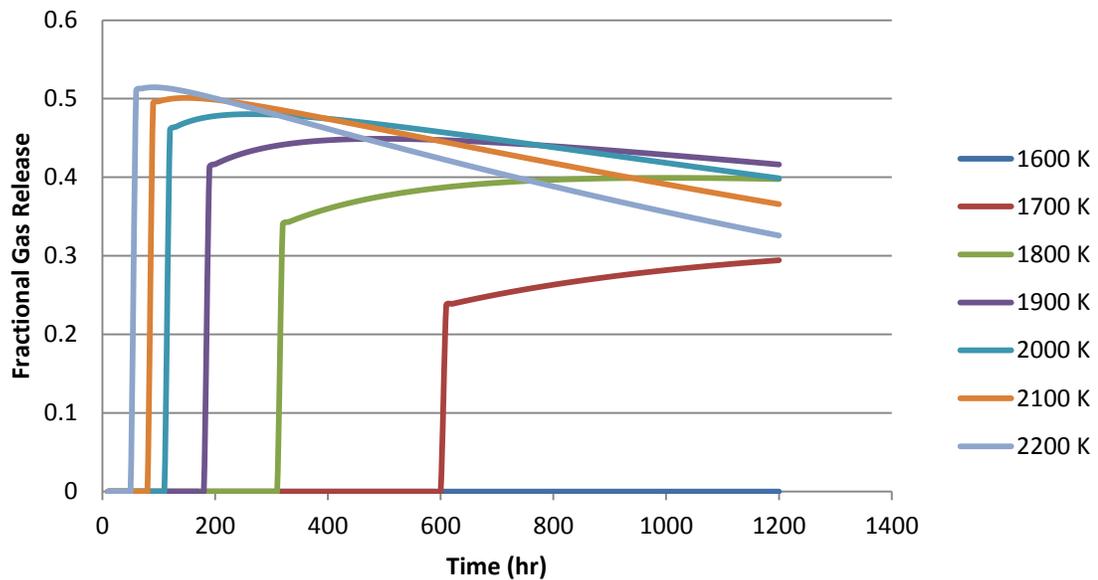


Figure 19. Fractional gas release over time (hr) for various temperatures (K) using Jernkvist and Massih's model of grain growth for UO_2 [17].

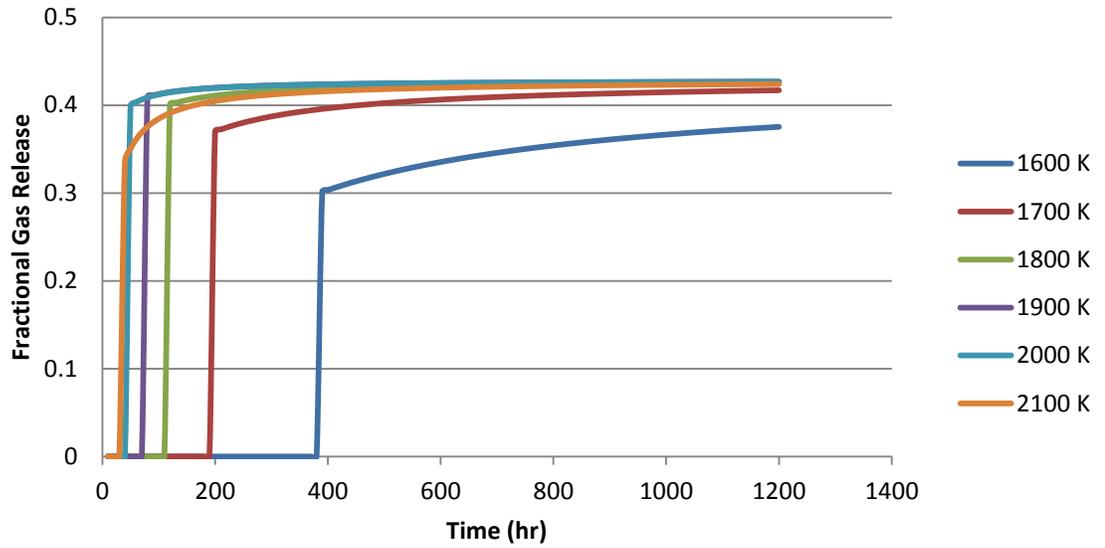


Figure 20. Fractional gas release over time (hr) for various temperatures (K) using Nichols' fourth power grain growth equation for MOX [23].

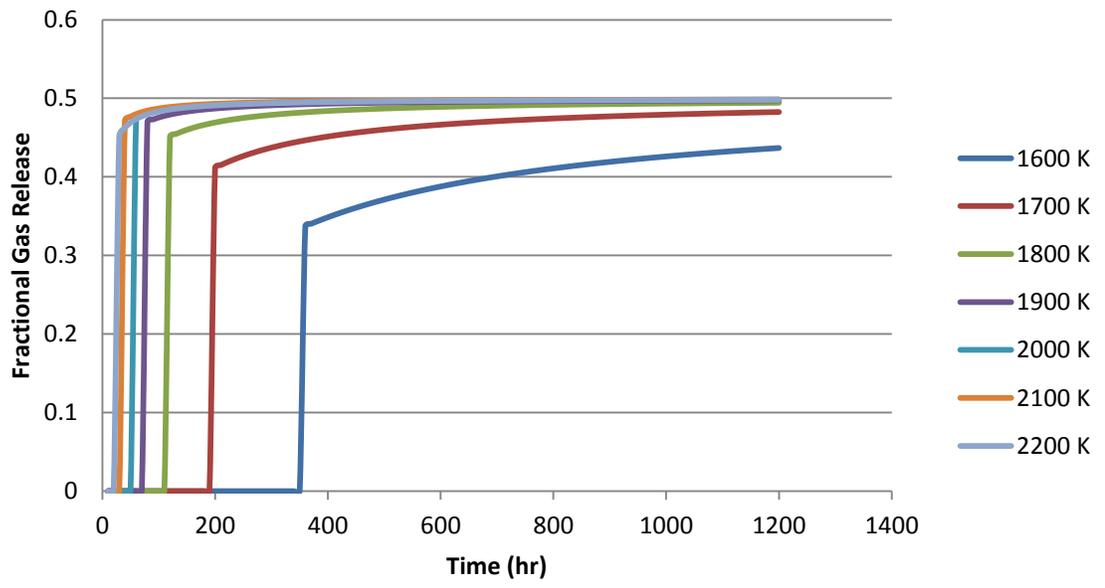


Figure 21. Fractional Gas Release over time (hr) for various temperatures (K) using Sari's cubic grain growth equation for MOX [24].

Figures 22, 23, and 24 show the fractional gas release of UO_2 and SBR MOX for a constant temperature of 1900 K and for varying initial grain radii. The gas release from UO_2 appears to behave in two different modes. In the declining mode, the gas release decreases from its peak once saturation occurs. In the rising mode, the gas release increases after saturation and appear to converge over time. The MOX fuel figures show the rising mode, except for the 9×10^{-6} m run with Nichols's grain growth model.

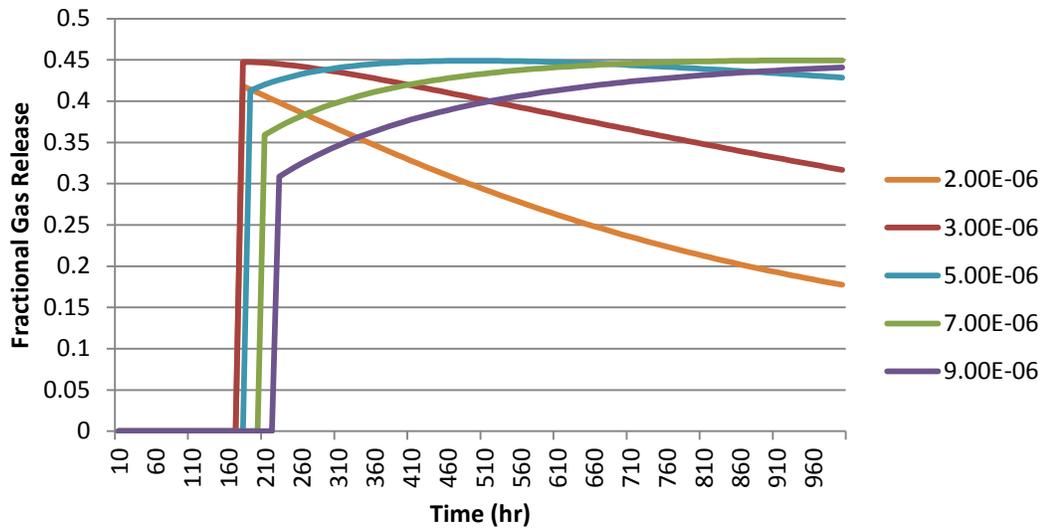


Figure 22. Fractional Gas Release over time (hr) for various Initial Grain Radii (m) using Jernkvist and Massih's model of grain growth for UO_2 [17].

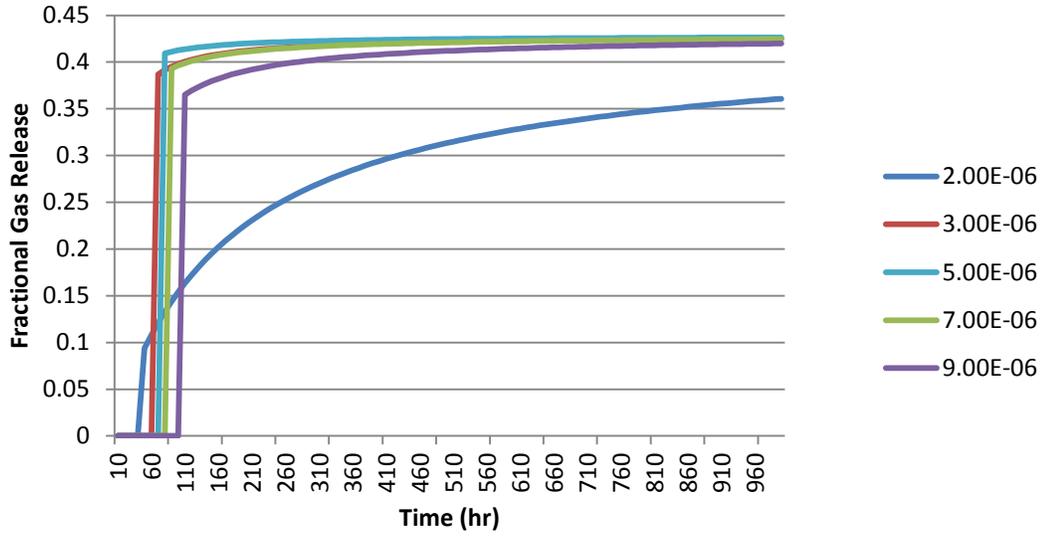


Figure 23. Fractional Gas Release over time (hr) for various Initial Grain Radii (m) using Nichols' fourth power grain growth equation for MOX [23].

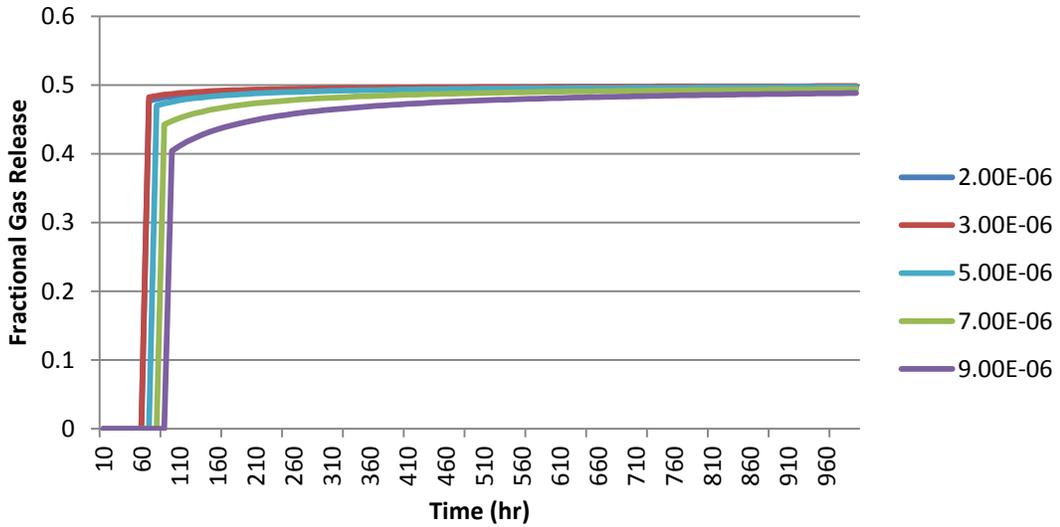


Figure 24. Fractional Gas Release over time (hr) for various Initial Grain Radii (m) using Sari's cubic grain growth equation for MOX [24].

The fuels used the previous figures use the same diffusivity coefficients, so they

only differ by temperature and rates of grain growth. Figure 25 shows the gas release of UO_2 for increased and decreased diffusivities D . Since the data was simulated with the model of continuous gas release, the complementary solution is set to zero, as seen in equation (66). Because of this, changing the diffusivity directly changes the magnitude of τ . An increase in τ leads to an increase in ${}_1e_0$ and ${}_2e_0$ as well as a decrease in Λ_1 and Λ_2 . There is no observable net change to the intergranular gas density, gaseous swelling, or fractional gas release.

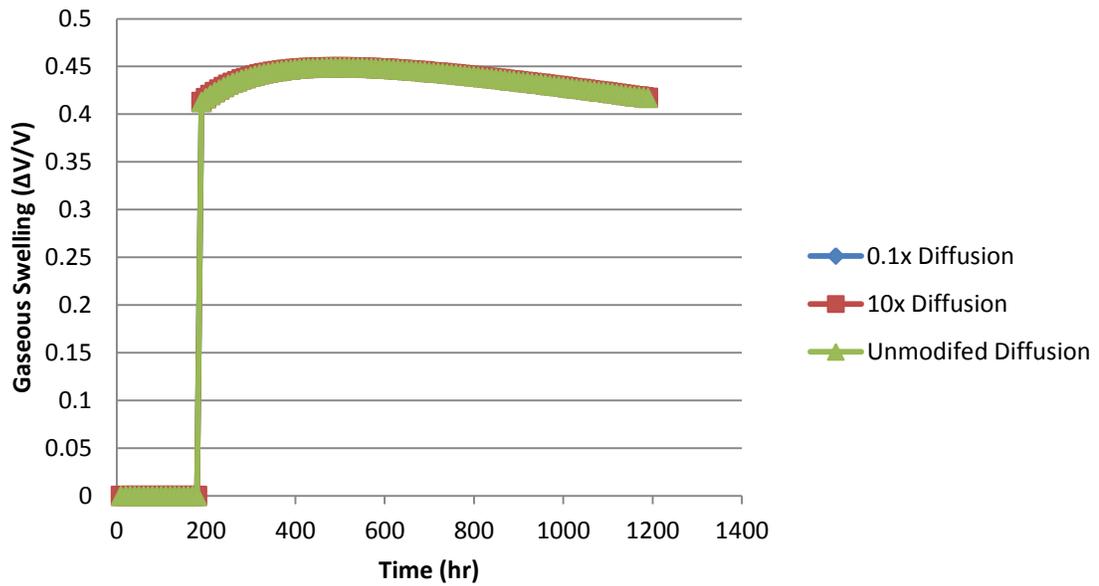


Figure 25. Fractional Gas Release over time (hr) from UO_2 at 1900 K for arbitrarily scaled diffusivities.

CHAPTER 5

CONCLUSION

In this work, the volumetric density of gas in intergranular bubbles is found from the diffusion of fission gas through fixed size and growing nuclear fuel grains. The values of this density are used to calculate the fractional gas release and the gaseous swelling of UO_2 fuel. It was shown that the swelling decreased at higher temperatures, which is related to the decreased total boundary surface area for larger grains of fuel. Figures 26 and 27 show that the gaseous swelling reaches its peak far faster than the fixed grain radius diffusion model, due to the grain boundary sweeping.

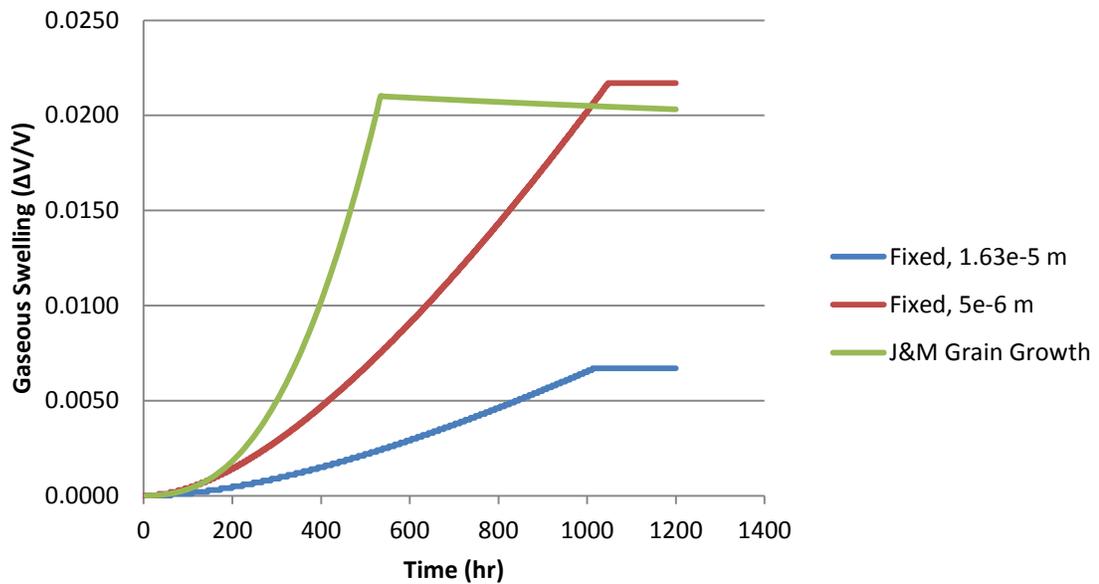


Figure 26. Gaseous Swelling over time (hr) for UO_2 at 1600 K. Fixed radius model simulated for the initial and final fuel grain radii (m) of the Grain Growth Model.

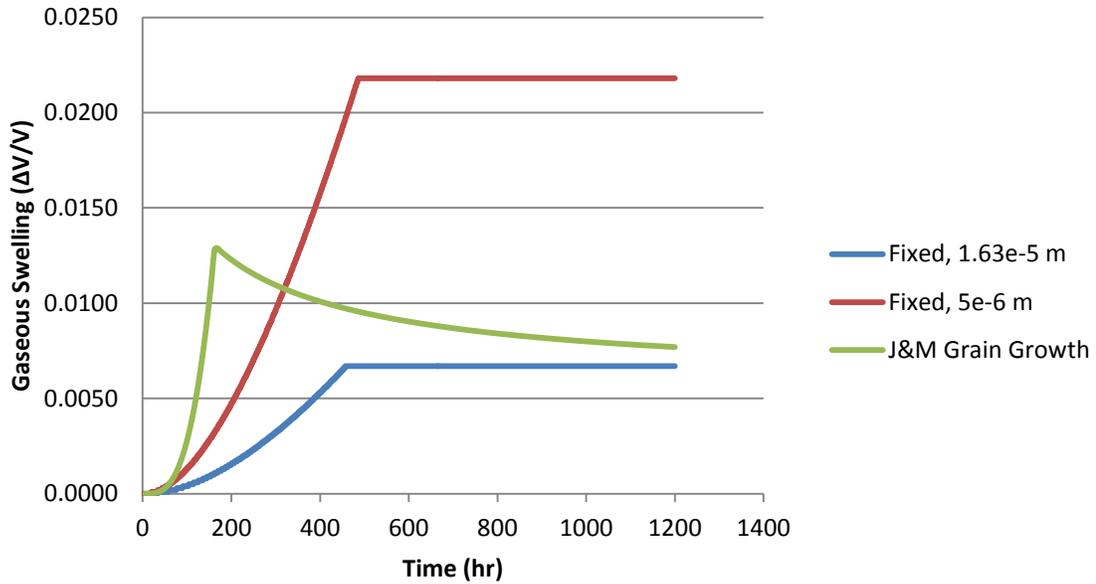


Figure 27. Gaseous Swelling over time (hr) for UO_2 at 1900 K. Fixed radius model simulated for the initial and final fuel grain radii of the Grain Growth Model.

Gas release and gaseous swelling of quasi-homogeneous SBR MOX fuel was also simulated. Due to the models of grain growth associated with MOX, the fractional gas release was found to converge to a single value for multiple temperatures. Gaseous swelling behaved similarly to that of UO_2 .

Currently, comparisons of grain growth to gas release for UO_2 and SBR MOX fuel are underrepresented in the published research. Schrire and Lysell [30] performed experiments that showed both sizable grain growth and increased fractional gas release in the center of a UO_2 fuel pellet in comparison to the rim. Fisher et al [18] have investigated the gas release from SBR MOX fuel, but only for peak temperatures of 1400 K. However, they noted that the gaseous swelling near the pin center was ~0.6% to ~1.2%, which falls within the range of the lower temperature MOX simulation runs. Data

that directly relates fission gas release to grain growth would be very beneficial.

Appendix A: Generalized Moment Weight Integrals

For the complementary solution, the generalized moment is as follows:

$$W_m \binom{0}{i f} = j_0 \frac{(\delta_i)}{R\mu_i(2R\mu_i - \delta_i)} \quad (\text{A.1})$$

$$W_m \binom{1}{i f} = \frac{[(R\mu_i)^{-1} + (2R\mu_i - \delta_i)^{-1}]j_0(\delta_i) + j_1(\delta_i)}{\omega_i(2R\mu_i - \delta_i)} \quad (\text{A.2})$$

$$W_m \binom{2}{i f} = \frac{v_0 + v_1 j_0(\delta_i) + v_2 j_1(\delta_i) + v_3 j_2(\delta_i)}{\omega_i^2(2R\mu_i - \delta_i)^2} \quad (\text{A.3})$$

$$\delta_i = R\mu_i - m\pi \quad (\text{A.4})$$

$$v_0 = 10 - \frac{2}{3}(R\mu_i)^2 \quad (\text{A.5})$$

$$v_1 = \delta_i [R\mu_i - 3(R\mu_i)^{-1} + (2R\mu_i - \delta_i)^{-1}] \quad (\text{A.6})$$

$$v_2 = 3(2R\mu_i - \delta_i) \quad (\text{A.7})$$

$$v_3 = \frac{4}{3}(2R\mu_i)^2 \quad (\text{A.8})$$

The generalized moment of the particular solution is given as

$$W_m \binom{0}{e_0} = w_m(1) \quad (\text{A.9})$$

$$W_m \binom{1}{e_0} = w_m(R^2) + 6\tau w_m(1) \quad (\text{A.10})$$

$$W_m \binom{2}{e_0} = w_m(R^4) + 20\tau w_m(R^2) + 60\tau^2 w_m(1) \quad (\text{A.11})$$

$$w_m(1) = (-1)^{m+1} (m\pi)^{-2} \quad (\text{A.12})$$

$$w_m(R^2) = R^2 (-1)^m (6(m\pi)^{-4} - (m\pi)^{-2}) \quad (\text{A.13})$$

$$w_m(R^4) = R^4 (-1)^m (-(m\pi)^{-2} + 20(m\pi)^{-4} - 120(m\pi)^{-6}) \quad (\text{A.14})$$

REFERENCES

- [1] D. R. Olander, *Fundamental Aspects of Nuclear Reactor Fuel Elements*. 1976 (Springfield, VA: National Technology Information Services).
- [2] M. O. Tucker, J. A. Turnbull, *Proc. R. Soc. Lond. A* **343** (1975) 290–314.
- [3] W. Beeré, G.I. Reynolds, The Morphology And Growth Rate Of Interlinked Porosity In Irradiated UO₂, *J. Nucl. Mater.* **47** (1973) 51.
- [4] R. Hargreaves, D.A. Collins, A Quantitative Model For Fission Gas Release And Swelling In Irradiated Uranium Dioxide, *J. Brit. Nucl. Energy Soc.* **15** (1976) 311.
- [5] K. Forsberg, A.R. Massih, Calculation Of Grain Boundary Gaseous Swelling In UO₂, *J. Nucl. Mater.* **377** (2008) 406.
- [6] K. Forsberg, A.R. Massih, Kinetics of Fission Product Gas Release During Grain Growth, *Modeling Simul. Mater. Sci. Eng.* **15** (2007) 335.
- [7] L. Vath, *J. Nucl. Mater.* **99** (1981) 324.
- [8] J.A. Turnbull, *J. Nucl. Mater.* **50** (1974) 62.
- [9] K. Forsberg, A.R. Massih, Diffusion Theory of Fission Gas Migration in Irradiated Nuclear Fuel, *J. Nucl. Mater.* **135** (1985) 140.
- [10] K. Forsberg, A.R. Massih, *J. Nucl. Mater.* **127** (1985) 137.
- [11] J.S. Rowlinson, B. Widom, *Molecular Theory of Capillarity*, Oxford University Press, Oxford, UK, 1982.
- [12] A. R. Massih, Message to H. Gibson. 05 Nov. 2012. E-mail.
- [13] M. V. Speight, *Nucl. Sci. Eng.* **37** (1969) 180.
- [14] J. A. Turnbull, C. A. Friskney, J. R. Findlay, F. A. Johnson, A. J. Walter, *J. Nucl. Mater.* **107** (1982) 168.
- [15] R. J. White, and M. O. Tucker, *J. Nucl. Mater.* **118** (1983) 1.
- [16] H. Matzke, *Radiat. Eff.* **53** (1980) 219.

- [17] L. O. Jernkvist, A. R. Massih, Models For Fuel Rod Behaviour At High Burn-Up Technical Report 2005:41 (Stockholm: Swedish Nuclear Power Inspectorate (SKI)) Available at: www.ski.se
- [18] S. B. Fisher, R. J. White, P. M. A. Cook, S. Bremier, R. C. Corcoran, R. Stratton, C. T. Walker, P. K. Ivison, I. D. Palmer, Microstructure of Irradiated SBR MOX Fuel and its Relationship to Fission Gas release, *J. Nucl. Mater.* **306** (2002) 153.
- [19] C.T. Walker, W. Goll, T. Matsumura, *J. Nucl. Mater.* **228** (1996) 8.
- [20] R.J. White, S.B. Fisher, P.M.A. Cook, R. Stratton, C.T. Walker, I.D. Palmer, *J. Nucl. Mater.* **288** (2001) 43.
- [21] R.J. White, in: International Seminar on Fission Gas Behaviour in Water Reactor Fuels, Cadarache, France, 26–29 September 2000, NEA/OECD, 2002, p. 189.
- [22] P. V. Uffelen, P. Botazzoli, L. Luzzi, S. Bremier, A. Schubert, P. Raison, R. Eloirdi, M. A. Barker, An Experimental Study of Grain Growth in Mixed Oxide Samples with Various Microstructures and Plutonium Concentrations, *J. Nucl. Mater.* **434** (2013) 287-290.
- [23] F.A. Nichols, *J. Appl. Phys.* **37** (1966) 4599.
- [24] C. Sari, *J. Nucl. Mater.* **137** (1986) 100.
- [25] Y. Long, L. J. Siefken, P. Hejzlar, E. P. Loewen, J. K. Hohorst, P. E. MacDonald, M. S. Kazimi, The Behavior of ThO₂-Based Fuel Rods During Normal Operation and Transient Events in LWRs, *Nuc. Tech.* **147** (2004) 120.
- [26] S. N. Laha, A. R. Das, Isothermal Grain Growth and Sintering in Pure ThO₂ and ThO₂-CaO Compositions, *J. Nucl. Mater.* **39** (1971) 285.
- [27] G.L. Hofman, *Nucl. Technol.* **47** (1980) 7.
- [28] G. Hofman, J. Snelgrove, B.R.T. Frost (Ed.), Metallic Fast Reactor Fuels, *Mater. Sci. Tech.* **10** (1994).
- [29] A.D. Whapham, On The Formation Of Gas Bubbles in Fissile Material During Reactor Irradiation, *Philo. Mag.* **185** (1971) 987.
- [30] D. Schrire, G. Lysell, Int. Topical Meeting on LWR fuel performance (European Nuclear Society Avignon, France, April 1991) 518.
- [31] A. Yu, S.P. Walker, R.T. Fenner, Pellet-Clad Bonding during PCMI, *Nuc. Eng. Design.* **121** (1990) 53.

- [32] K. H. Neeb, *The radiochemistry of nuclear power plants with light water reactors*, New York :De Gruyter, 1997, p210.
- [33] F. J. Humphreys, M. Hatherly, *Recrystallization and Related Annealing Phenomena*. Pergamon : Oxford, 1995.
- [34] A. H. Booth, Atomic Energy of Canada Limited Report. **496** (1957).
- [35] J. R. Matthews, M. W. Wood, An Efficient Method for Calculating Diffusive Flow to a Spherical Boundary, *Nuc. Eng. Design.* **56** (1980) 439.
- [36] P. T. Elton, K. Lassmann, Calculational Method for Diffusion Gas Release, *Nuc. Eng. Design.* **101** (1987) 259.
- [37] M. Abramowitz, I. A. Stegun, *Handbook of Mathematical Functions*, New York: Dover, 1964.
- [38] D. Davies, G. Long, AERE Rep. No. 4347 (1963).
- [39] A.W. Schilling, Unpublished work , (1964).
- [40] J. E. Burk, D. Turnbull, *Prog. Met. Phys.* (1952) 3220–92.